AZƏRBAYCAN MİLLİ ELMLƏR AKADEMİYASI

AZƏRBAYCAN ASTRONOMİYA JURNALI

2017, Cild 12, № 2

AZERBAIJAN NATIONAL ACADEMY OF SCIENCES

ASTRONOMICAL JOURNAL OF AZERBAIJAN

2017, Vol. 12, No. 2

Bakı-2017 / Baku-2017

ASTRONOMICAL JOURNAL OF AZERBAIJAN

Founded in 2006 by the Azerbaijan National Academy of Sciences (ANAS)
Published in the Shamakhy Astrophysical Observatory (ShAO) named after N. Tusi, ANAS
ISSN: 2078-4163 (Print), 2078-4171 (Online)

Editorial board

Editorial Office address:	ANAS, 30, Istiglaliyyat Street, Baku, AZ-1001, the Republic of Azerbaijan
Address for letters:	ShAO, P.O.Box №153, Central Post Office, Baku, AZ-1000, Azerbaijan
E-mail:	aaj@shao.az
Phone:	(+994 12) 510 82 91
Fax:	(+994 12) 497 52 68
Online version:	http://www.aaj.shao.az

ASTRONOMICAL JOURNAL OF AZERBAIJAN

2017, Vol. 12, № 2

Contents

ON ONE PROBLEM IN SOLAR WIND PHYSICS

N. S. Dzhalilov*

Shamakhy Astrophysical Observatory named after N.Tusi,
Azerbaijan National Academy of Sciences, Shamakhy region, Azerbaijan

In recent years, intensive researches have been carried out to be clarified properties of the temperature anisotropy of the solar wind plasma. The results of numerous satellite measurements of solar wind parameters at various distances from the Sun revealed a special form of distribution of the rate of temperature anisotropy. However, not all aspects of this distribution can be understood and modeled theoretically. In this paper, we give a brief literature review on the results achieved in solving this problem.

.

1. INTRODUCTION

The solar wind models should describe the physical mechanism of plasma acceleration in the solar corona, the generation of plasma outflow at supersonic speed, the formation of the heliosphere, and support of the supersonic flow velocity to the edge of the heliosphere. Describing the global structure of the heliosphere as a whole, the model should correctly describe the physical variables that are well known from measurements near the Earth on the plane of the ecliptic and on the solar corona. An intensified experimental study of the properties of the plasma of the solar wind near the Earth and its modeling are associated, first of all, with the diagnostic problems of space weather. Any fluctuations in the flow of wind affect the Earth magnetosphere, causing changes in the condition of the occurrence of magnetic storms and so variations of parameters of the upper atmosphere and ionosphere. Let us briefly consider the development directions of solar wind modeling.

In a total solar eclipse, the visible white corona (due to Thomson scattering effect of photosphere light from thefree electrons in a fully ionized corona) stretches to about 10 R (R is the radius of the Sun). In 1942, Edlen [1] proved that such an expanded corona is heated to $T_e \approx 10^6 K$. Since then, the cause of the heating of

* E-mail: namigd@mail.ru

the solar corona plasma has become one of the unsolved fundamental problems of the physics of the Sun. At that time, the radial distribution of the brightness of the corona was well described by the electron density profile, and the temperature was assumed to be constant. Thus, for a long time the idea that the corona is static, isotropic and has a very high thermal conductivity has beendominated one [2]. For the first time in 1957, Chapman [3] abandoned the isotropic approximation, still believing that in the corona the condition of hydrostatic equilibrium was fulfilled globally. He obtained a temperature profile that tends to zero at infinity. However, such a profile corresponded to the density, which after a distance of 174 R starts to grow. This meant that the solution found was unstable. Parker, analyzing the conclusions of the hydrostatic model, came to the conclusion that the corona should expand [4]. He proceeded from the fact that the hydrostatic model at infinity gives a finite value of pressure and density, which far exceed the pressure and density of the interstellar medium. This imbalance of pressure should lead to an expansion of the corona. He first constructed a hydrodynamic model of the solar wind, showing that, because of the high temperature, the gas pressure gradient is so large that the plasma can accelerate to supersonic speed [5, 6]. Parker's theory explained the experimental data on the deviation of the comet's tail as it comes near the Sun [7] and found confirmation of the existence of a supersonic stream from the sun in numerous space experiments, beginning with the Soviet space experiment Luna-1 (1959) and Mariner-2 [8]. After Parker's work, modeling of the solar wind, including various aspects of thismatterwas intensively developed. Numerous works were devoted to such questions as the wind with many-fluid components, nonradial expansion, nonstationary models, consideration of nonidealeffects, collisional and collisionless kinetic models, and many others. An overview of these models can be found, for example, in [9, 10]. There are two basicallydifferent approaches to modeling the solar wind: MHD and kinetic models. Kinetic models solve equations for the particle velocity distribution functions, and the MHD models solve the equations for the integral moments of these functions. Thus, the foundations of both approaches are the same - the Boltzmann and Maxwell equations. Each of the approaches, however, has its advantages and disadvantages [11]. However, it should be noted that the values extracted from the experiments are mainly macroscopic (flow velocity, mass flow density, temperature, magnetic field, etc.).

Modern simulation models consist of two interconnected parts: internal (coronal) and external (heliospheric). The coronal part of the model uses magnetic synoptic charts of the solar photosphere as input parameters and extrapolates them to the surface of the heating source, which is at a distance of approximately 2.5 R. Then the physical parameters of the corona are calculated to distances (20 ± 30) R [12]. The obtained boundary values of this part of the model are

applied as initial values for the heliospheric part of the model and the calculation is carried out to a distance of 1 AU and more. However not all the observed data are successfully described by such models.

On the basis of numerous observed facts and theoretical simulations, it became clear that the main basic parameters of the solar wind are established in the region of wind formation, where the velocities are all still subsonic. The chemical composition of the wind takes its origin from the chromospheric layers [13], and the acceleration region is only a few radius away from the Sun [14–16], which indicates that the source of the heat flux carried by the wind is in the corona. The density of the mass flux of the solar wind is formed at the level of the transition zone between the corona and the chromosphere [17]. Thus, the wind formation region covers both the collisional plasma in the lower layers of the solar atmosphere and the almost collisionless plasma in the upper corona. This means that theparticles distribution functions of the plasma, especially for protons and other heavy ionspasses with height from the Maxwellian form to the non-Maxwellian function. Modeling the formation of wind in such an environment, where isotropic plasma with altitude sharply turns into an anisotropic one, meets with serious difficulties. With distance, the density decreases rapidly and external effects (expansion of the flow, magnetic, electric and gravitational forces, interaction of waves with particles, etc.) increase the anisotropy of the solar-wind plasma.Measurements of the temperature of protons and oxygen ions in the flow from coronal holes on the satellite SOHO indicate that strong anisotropy arises even in the corona itself [18]. Further all satellite measurements showed that protons and ions far from the Sun are strongly anisotropic, and the rate of anisotropy for electrons is small, see, for example, in [19]. While the constructed models describe the basic structural elements and the basic parameters of the wind (velocity, temperature, mass flow, magnetic field)as a whole, important questions remain open. For example, whythe protons and alpha particles in the accelerated component of the solar wind coming from coronal holes aremore heated than electrons? Next we will concentrate on the anisotropy of the solar wind plasma.

2. ANISOTROPY OF THE SOLAR WIND PLASMA

The solar-wind plasma is an almost collisionless anisotropic medium. For example, at the distance of 1 AU from the Sun, the mean free path of electrons is of the order of 108 km, which is comparable to the size of the system itself. The presence of an external magnetic field is the main obstacle to the isotropization of such plasma. The temperature anisotropy of the plasma (parallel $T_{\|}$ and perpendicular $T_{\perp}$ values with respect to the direction of the magnetic field differ) is well established fact from the experiments [20–22]. It can occur due to the effects of

wind expansion [23], resonant wave-particle interaction [24], ion capture (pickup ions) [25], shear flows [26], and many other compression and expansion effects. The rate of anisotropy varies depending on the type of particles (electrons, protons, alpha particles and other ions) and, it is different in different components of the solar wind (fast, slow, CME, etc.) [21, 27]. In most cosmic experiments, the temperature of the particles and the magnetic field of the solar-wind plasma are directly measured parameters. Such measurements are concentrated mainly on the range of distance from 0.3 to 4.0 AU in the plane of the ecliptic, which allow to study the radial changes of the measured parameters [28]. Numerous measurements yield results on the rate of anisotropy in the plane $(T_\perp/T_\parallel, \beta_\parallel)$ for both protons and electrons. It turned out that the distribution of the rate of anisotropy $T_\perp/T_\parallel$ as a function of $\beta_\parallel$(the plasma beta along the magnetic field - the ratio of the parallel ion or electron gas pressure to the magnetic field pressure) has a limited rhomboid shape with sharp boundaries [27, 29, 30]. For example, a typical example of the distribution of the rate of anisotropy as a function of $\beta_\parallel$in a slow solar wind is shown in Fig. 1 for protons [29] and Fig. 2 for electrons [21].

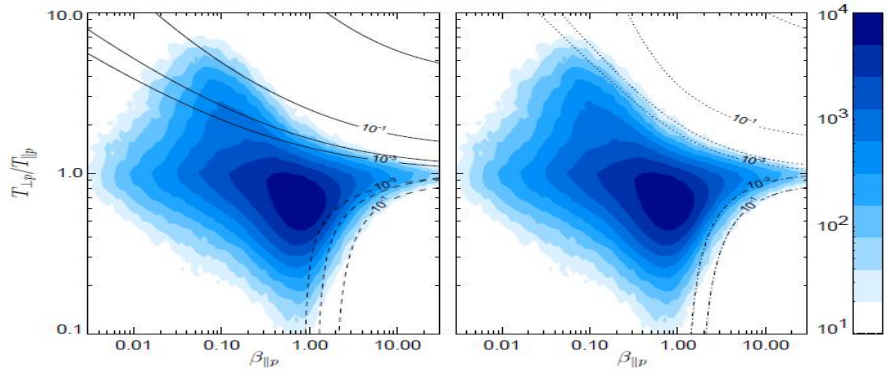

Fig. 1. The distribution of the rate of proton temperature anisotropy as a function of plasma beta $\beta_{\parallel p}$ in a slow solar wind ($V < 600$ km s^-1) according to the measurements in the satellite WIND/SWE (1995-2001). The color area is measured values, and their gradient determines (with a logarithmic scale shown on the right side) the measurement frequency. The theoretical contours of the maximum of the instability growth rate normalized to the proton cyclotron frequency Ω_p are plotted over the experimental data. Left: solid curves - growth rates of cyclotron instability, dashed lines - growth rates of parallel fire hose instability. Right: dotted curves – mirror instability and dash-dotted curves - growth rates of the second oblique fire hose instability (the pictures were taken from [29]).

Theoretical explanation of the boundaries of such distributions became the important problem in the physics of the solar wind. The solution of this problem

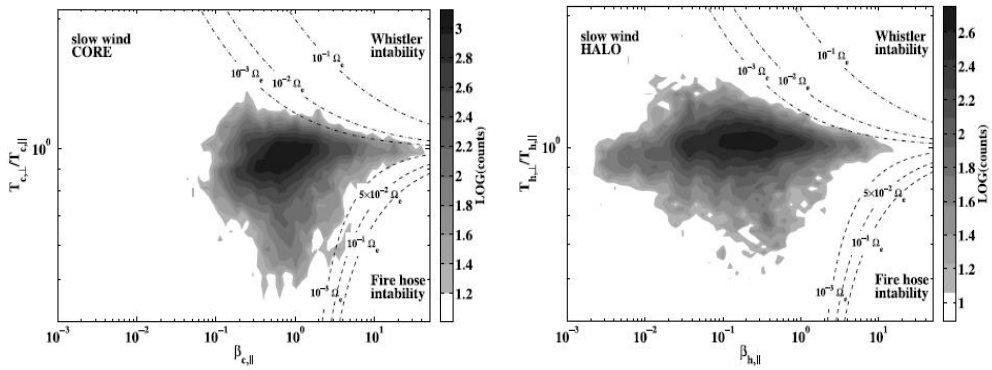

Fig. 2. Distribution of the rate of electron anisotropy in the slow wind. The pictures on the left and on the right side correspond to the core and halo populations in the electron velocity distribution functions. The overdrawn curves correspond to the isocontours of the maximum growth rate of the kinetic fire hose and whistler instabilities at the unit of the electron cyclotron frequency (the pictures are taken from [21]).

will make it possible to understand, as a result of which mechanisms the isotropic plasma on the Sun, leaving its limits, becomes anisotropic at a distance of several AU with known distribution boundaries? Clarification of this question may provide a clue for understanding such mechanisms as particle acceleration and solar wind generation, support of supersonic velocity to the edge of the heliosphere, explanation of the generation of the observed low-frequency turbulence, and its role as a source of energy to support particle velocity and many others. If we do not involve any physical mechanism capable of redistributing the energy between the transverse and longitudinal thermal motions of the particles, then the classical CGL law [31] of the adiabatic expansion of the solar wind along the spiral of the interplanetary magnetic field, predicts an excessively high degree of temperature anisotropy with $T_{\parallel}/T_{\perp} > 1$. For example, in a slow wind in 1 AU for the electron temperature anisotropy should be $T_{\parallel}/T_{\perp} > 30$ [32]. However, the observed values of the temperature anisotropy of electrons are near unity [21, 33, 34]. The main mechanism for explaining such discrepancies and observed $(T_{\perp}/T_{\parallel}, \beta_{\parallel})$ distribution boundaries is plasma isotropization by plasma instabilities [35], which arise due to the pressure anisotropy in a plasma with non-Maxwellian particle distribution functions [36–38]. It is generally accepted that the main mechanism leading to an inverse anisotropy with $T_{\parallel}/T_{\perp} < 1$ is cyclotron resonance of particles [39].

Theoretical simulations of instabilities in the non-Maxwellian plasma were developed, mainly in the kinetic approximation, using the Vlasov equations for the particle velocity distribution functions and the Maxwell equations for the electromagnetic field. The results of the investigations show that the temperature

anisotropy of the plasma at large scales initiates, first of all, the excitation of fire hose and mirror instabilities [23, 40–44] both in the ion and in the electron components. Fire hose instability, arising as growing of Alfvén waves, is non-resonant in nature [23, 45, 46] and its saturation occurs as the result of particle scattering [47]. The compressible mirror modes are kinetic by nature and their saturation occurs as a result of resonant capture of particles [48, 49]. Among the various instabilities that are excited due to temperature anisotropy, fire hose instability is considered to be dominant. It occurs if the parallel temperature is greater than perpendicular. In the conditions of the solar and stellar wind, such a premise is easily realized [50]. In the expanding plasma, the condition for the conservation of the magnetic moment of the particles requires the fulfillment of the $T_{\|}/T_{\perp} > 1$.

The spectrum of small-scale instabilities of anisotropic plasma is more diverse [51]. As shown, for example in [21, 52, 53], electrons with $T_{\perp} > T_{\|}$ fall into a cyclotron resonance with parallel whistler modes with a frequency $\Omega_p < \omega < \Omega_e$ velength of which is in order of the electron inertial length (c/ω_{pe}). In the opposite case, when $T_{\perp} < T_{\|}$ the electron fire hose [55] and the second (oblique) electron fire hose instabilities are excited. In this case, the electrons and protons are in resonance, and the growth rate of the instability depends also from the proton temperature.

Similar calculations for explanation of the observed proton anisotropy were carried out in a number of works, for example, in [20, 29, 56]. In a proton plasma with a temperature $T_{\perp p} > T \|$, cyclotron [52, 57] and mirror instabilities arise [40, 58, 59]. In the case of $T_{\perp p} < T_{\| p}$, parallel [60] and oblique fire hose [61] instabilities are preferable. The proton cyclotron instability is resonant by nature and occurs in cyclotron waves with a frequency $\omega < \Omega_p$ propagating along the magnetic field. The proton mirror instability in the reference system of the plasma has zero frequency ($\omega = 0$), and the wave vector is directed at an angle to the magnetic field. Mirror modes create regions of magnetic field depression or mirrors for particles, as a result of which particles trapped in these regions are in resonance with the wave [62]. Because of the excess of the transverse pressure inside the mirror, the transfer of the kinetic energy of the particles to the wave causes the growth of mirror instability [48]. According to the results of the linear kinetic theory, the mirror instability dominates at high $\beta_{\|}$, and the cyclotron instability at relatively low $\beta_{\|}$ [63]. Proton mirror instability is often observed in various objects: Earth's magnetosheath [64], solar wind [65], comets [66], in the magnetosheaths of other planets like Jupiter and Saturn [67, 68], and in the heliosheath [69]. According to the theory, the proton cyclotron instability should be dominant at relatively low $\beta_{\|}$. However, in observations, the appearance of mirror modes in this region is interpreted by suppressing cyclotron instability by the presence of heavy ions [70].

The importance of the role of fire hose instability for isotropization of protons [30, 71, 72], electrons [21] and alpha particles [73, 74] is directly proved in *situ* observations. Historically, fire hose instabilities were investigated in the MHD approximation as instability of low-frequency Alfvén waves [23, 75, 76]. Later, in many works hose modes arising due to the anisotropy of proton and electron components were studied in the kinetic approximation, for example in [55,77–81]. Because of the kinetic effects, both fire hose modes have a finite frequency, and their instability growth rates reaches a maximum in the case of parallel propagation. Despite the fact that under the same plasma conditions the classical incompressible parallel fire hose instability on Alfvén modes is preferable (it is easily generated, has more growth rate, has more amplitude in the nonlinear stage, etc.) than the compressible oblique fire hose instability in slow magnetosonic modes [82], the advantage is given to oblique modes. This is because the instability threshold of the proton oblique fire hose mode is better suited to explain the boundaries of $(T_\perp/T_\parallel, \beta_\parallel)$ distributions for $\beta_\parallel > 1$ [27].

It should be noted that in the Vlasov's linear kinetic theory, the electron anisotropy is not taken into account in studying the distribution of anisotropy rate of protons, and conversely, the electron anisotropy is investigated for isotropic ions. This is done to simplify mathematical calculations, taking into account that the contributions of anisotropy of other particles are negligible due to the independence of physical mechanisms leading to anisotropy of electrons and ions [28]. However, in [83, 84], the criterion for the appearance of parallel hose instability was investigated under conditions when both components of the plasma are anisotropic. As a result, the authors obtained an instability threshold modified by the anisotropy of the electrons, which much better explains the boundaries of the $(T_\perp/T_\parallel, \beta_\parallel)$ distribution for protons. The cumulative effects of the anisotropy of protons and electrons on the basis of the bi-Maxwell and bi-kappa distributions were studied in [28,85]. Comparing the results with observations, the authors concluded that it is important to take into account electron anisotropy. In [86, 87], it was shown that the anisotropy of electrons suppresses the growth of proton cyclotron instability, and significantly enhances mirror instability [88, 89]. The mirror structures observed in magnetosheath are explained by these processes. The role and influence of the anisotropy of alpha particles to the fire hose instability and in its nonlinear evolution was investigated in [90]. To the best of our knowledge, until now, within the framework of the kinetic and MHD theories, the boundaries of the $(T_\perp/T_\parallel, \beta_\parallel)$distributions for $\beta_\parallel < 1$ remain unexplained.

In the dynamics of weakly collisional plasma, especially in transport phenomena, the role of low-frequency kinetic instabilities associated with thermal anisotropy (the mirror, ion-cyclotron, fire hose instabilities) is important for the macroscopic evolution of cosmic and astrophysical systems [50]. For example, the

role of these instabilities was studied in accretion disks [91–94], in a hot plasma cluster of galaxies [95,96], in magnetic reconnection [97–100], etc.

Due to the fact that the measured plasma parameters are macroscopic, the MHD description of the plasma is more appropriate. The derivation of closed MHD equations for the collisionless plasma has its difficulties. The main difficulty is due to the interruption of chains of infinite equations for the moments of the distribution functions. This requires additional physical justification, and a specific form of the particle velocity distribution function is required. Classical examples of such equations describing plasmas as a fluid are CGL [31] and 16-moment transport equations [101, 102] derived for the Bi-Maxwellian plasma at zero Larmor radius. The main advantage of the 16-moment MHD transport equations in comparison with the CGL-equations is that these equations take into account the heat flux along the magnetic field. Unlike the CGL equations, the 16-moment equations give the correct expression for the criterion for the appearance of mirror instability, which coincides with the low-frequency kinetic result [103, 104]. MHD plasma descriptions in comparison with kinetics have a significant drawback, which is that small wave numbers, $k < \omega_{pp}/c$, are considered. In a number of works, estimates of the modification of the MHD instabilities were carried out when the finite length of the Larmor radius was taken into account [105, 89].

CONCLUSIONS

In previous papers we developed the theory of MHD instabilities based on 16-moment equations [103–107]. In those papers, the results were obtained for ion plasma. The role of the electrons was reduced only to ensure the quasineutrality of the plasma. Strictly speaking, ignoring the contributions of the electronic component of the plasma requires the condition $T_e << T_p$, which in realistic situations can occur only under special conditions. In connection with the problems described above, we began to generalize the theory of MHD instabilities including electronic component and its anisotropy.

In conclusion, we note that near 1 AU the solar-wind plasma has $(T_\perp/T_\parallel, \beta_\parallel)$ distribution like to rhomboid shape. In general, low-frequency kinetic instabilities describe the boundaries of this distribution quite well for $\beta_\parallel > 1$, both for the electron and ionic components of the plasma. However, there are still a number of open questions. For example, the threshold value of the maximum of the instability growth rate has a certain value, but its essence is not clear. In the discussed issue, the most important feature is simulation of the observed boundaries of the distribution of the rate of temperature anisotropy for $\beta_\parallel < 1$. So far the answer to this question has not been found in the kinetic approach. However, in the

MHD approach, when anisotropic heat flux along the magnetic field is taken into account, new types of instabilities arise. We showed this earlier in the example of proton plasma [103, 104, 106, 107]. In the future, we plan to generalize these results, taking into account anisotropy of the electronic component and, possibly, alpha particles. We think that the having a new types of instabilities associated with heat flow, we have a chance to solve the problem under discussion.

ACKNOWLEDGMENTS

We acknowledge grants from Science Development Foundation under the President of the Republic of Azerbaijan - Grant number EIF-KETPL-2-2015-1(25)-56/11/1.

REFERENCES

1. Edlén B An attempt to indentify the emission lines in the spectrum of the solar corona.Arkiv for MMareMatik Astronomi, o Fysik, 1942, 28B(1), 1-4

2. Van de Julst H. The chromosphere and corona.In:Kuiper G.(ed) The Sun, 1953, University of Chicago, 307-321

3. Chapman S. Notes on the solar corona and the terrestrial ionosphere, Smithson ContribAstrophys, 1957, 1-12.

4. Parker E. Dynamics of the interplanetary gas and magnetic fields.Astrophys J., 1958, 128, 664-676

5. Parker E. Interplanetary dynamical processes.Interscience , 1963 , New York.

6. Parker E. Dynamical properties of stellar coronas and stellar winds.iv.The separate existence of subsonic and supersonic solutions.Astrophys J., 1965, 141, 1463-1478.

7. Biermann L., Physical processes in comet tails and their relation to solar activity. Mém. Soc. Roy. Sci. 1953, Liège (Ser 4), 13, 291.

8. Neugebauer M., Snyder C. Solar plasma experiment. Science, 1962, 138, 1095–1097.

9. Marsch E, Theoretical models for the solar wind, Advances in Space Research, 1994, 14, 103 /DOI:10.1016/0273-1177(94)90170-8.

10. Marsch E. Kinetic physics of the solar corona and solar wind. Living Rev. Solar Phys. 2006, 3 / URL: http://www.livingreviews.org/lrsp–2006–1.

11. Parker E. Kinetic and Hydrodynamic Representations of Coronal Expansion and the Solar Wind. Twelfth International Solar Wind Conference, 2010, 1216, 3–7 / DOI: 10.1063/1.3395887.

12. Riley P., Linker J.A., Miki_Z. An empirically-driven global MHD model of the solar corona and inner heliosphere. J. Geophys. Res. 2001, 106, 15889 -15902, DOI:10.1029/2000JA000121.

13. H'enoux J.C. FIP fractionation: Theory. Space Science Reviews, 1998, 85, 215–226, DOI 10.1023/A: 1005194215611

14. Habbal S.R., Esser R., Guhathakurta M., Fisher R.R. Flow properties of the solar wind derived from a two-fluid model with constraints from white light and in situ interplanetary observations. Geophys. Res. Lett. 1995, 22(12), 1465-1468.

15. Grall R.R., Coles W.A., Klinglesmith M.T., Breen A.R., Williams P.J.S., Markkanen J., Esser R. Rapid acceleration of the polar solar wind. Nature, 1996, 379, 429-432.

16. Antonucci E., Dodero M.A., Giordano S. Fast solar wind velocity in a polar coronal hole during solar minimum. Solar Phys. 2000, 197, 115-134.

17. Lie-Svendsen., Leer E., Hansteen V.H. A 16-moment solar wind model: From the chromosphere to 1 AU. J. Geophys. Res., 2001, 106, 8217-8232.

18. Cranmer S.R., et al. An empirical model of a polar coronal hole at solar minimum. Astrophys. J. 1999, 511, 481-501.

19. 19. Marsch E., MuM"uhlh"auser K.H., Schwenn R., Rosenbauer H., Pilipp W., Neubauer F.M. Solar wind protons - Three-dimensional velocity distributions and derived plasma parameters measured between 0.3 and 1 AU. J. Geophys. Res., 1982, 87(A1), 52-72.

20. Kasper J. C., Lazarus A. J., Gary S. P., Szabo A. Solar wind temperature anisotropies, in: Solar Wind Ten, edited by M. Velli et al., AIP Conf. Ser., 2003, 679, 538– 541.

21. S'tvera'k S'., Tra'vnn;'c'ek P., Maksimovic M., Marsch E., Fazakerley A.N.,Scime E.E. Electron temperature anisotropy constraints in the solar wind. J. Geophys.Res., 2008, 113, A03103 / DOI:10.1029/2007JA012733.

22. Hundhausen A. J., Asbridge J. R., Bame S. J., Gilbert H. E., Strong I. B., Vela 3 Satellite Observations of Solar Wind Ions: A Preliminary Report, JGR, 1967, 72, 87.

23. Parker E. N. Dynamical Instability in an Anisotropic Ionized Gas of Low Density. Ph.Rv., 1958, 109, 1874.

24. Cranmer S.R. Ensemble Simulations of Proton Heating in the Solar Wind via Turbulence and Ion Cyclotron Resonance. Ap. J. S., 2014, 213, 16.

25. Isenberg P.A. Interstellar pickup ions: Not just theory anymore. RvGeS, 1995, 33, 623.

26. Schekochihin A.A., Cowley S.C., Kulsrud R. M., Rosin M.S., Heinemann T. Nonlinear Growth of Firehose and Mirror Fluctuations in Astrophysical Plasmas, Ph. Rv. L., 2008, 100, 081301.

27. Chen C.H. K., Matteini1 L., Schekochihin A.A., Stevens M.L., Salem C.S., Maruca B.A., Kunz M.W., Bale S.D. Multi-species measurements of the firehose and mirror instability thresholds in the solar wind. Astrophys. J. Letters, 2016, 825, L26.

28. Shaaban S.M., Lazar M., Poedts S., Elhanbaly A. Shaping the solar wind temperature anisotropy by the interplay of electron and proton instabilities, arxiv:1612.01012v1 [astro-ph.SR] 3 Dec 2016.

29. 29. Hellinger P., P. Tra'vnı'e'ekJ. C. Kasper, Lazarus A. J. Solar wind proton temperature anisotropy: Linear theory and WIND/SWE observations. Geophys. Res. Lett., 2006, 33, L09101/DOI:10.1029/2006GL025925.

30. Bale S.D., Kasper J.C., Howes G.G., et al. Magnetic Fluctuation Power Near Proton Temperature Anisotropy Instability Thresholds in the Solar Wind. Ph. Rv. L, 2009, 103, 211101.

31. Chew G.F., Goldberger M.L., Low F. E. The Boltzmann equation and the one-fluid hydromagnetic equations in the absence of particle collisions. Proc. R. Soc., London, 1956, 236, 112-118.

32. Phillips J.L., Gosling J.T. Radial evolution of solar wind thermal electron distributions due to expansion and collisions. J. Geophys. Res., 1990, 95, 4217-4228.

33. Feldman W., Asbridge J.R., Bame S.J., Montgomery M.D., Gary S.P. Solar wind electrons. J. Geophys. Res., 1975, 80, 4181-4196.

34. Pilipp W.G., Muehlhaeuser K.-H., Miggenrieder H., Rosenbauer H., Schwenn R. Variations of electron distribution functions in the solar wind. J. Geophys. Res., 1987, 92, 1103-1118.

35. Gary S.P. Theory of Space Plasma Microinstabilities, Cambridge Univ. Press, 1993 (reprinted 2005).

36. Eviatar A., Schulz M. Ion-temperature anisotropies and the structure of the solar wind. P&SS,1970, 18, 321

37. Gary S.P., Montgomery M.D., FeldmanW.C.,Forslund D.W. Proton temperature anisotropy instabilities in the solar wind. J. Geophys.Res., 1976, 81, 1241.

38. Gary S.P., Jian L.K., Broiles T.W., Stevens M.L., Podesta J.J., Kasper J.C., İon-driven instabilities in the solar wind: Wind observations of 19 March 2005, J. Geophys. Res., Space Physics, 2016, 121(1), 30.

39. Hollweg J.V., Isenberg P.A. Generation of the fast solar wind: A review with emphasis on the resonant cyclotron interaction. J. Geophys.Res., 2002, 107, 1147.DOI: 10.1029/2001JA000270.

40. Chandrasekhar S., Kaufman A. N., Watson K.M. The stability of the pinch. Proc. R. Soc. Lond.Ser.A, 1958, 245, 435-455.

41. Vedenov A.A./Sagdeev R.Z. in: Plasma Physics and the Problem of Controlled Thermonuclear Reactions, Ed.BY M.A.Leontovich (Izd.Akad.Nauk SSSR, Moscow, 1958;Pergamon, New York, 1959), Vol.3, 278 p.

42. Hasegawa A. Drift mirror instability of the magnetosphere. Ph.Fl., 1969, 12, 2642.

43. Rudakov L.I., Sagdeev R.Z. in: Plasma Physics and the Problem of Controlled Thermonuclear Reactions, Ed.by M. A. Leontovich (Izd. Akad. Nauk SSSR, Moscow, 1958; Pergamon, New York, 1959), Vol. 3, p. 321.

44. Vedenov A.A., Sagdeev R.Z. Plasma Physics and the Problem of Controlled Thermonuclear Reactions, Ed.by M. A. Leontovich (Izd. Akad. Nauk SSSR, Moscow, 1958; Pergamon, New York, 1959), Vol. 3, p. 332.

45. Pilipp W., Volk H. J. Analysis of electromagnetic instabilities parallel to the magnetic field. J. Plasma Phys., 1971, 6, 1.

46. Wang B.-J., Hau L.-N. MHD aspects of fire-hose type instabilities. J. Geophys.Res., 2003, 108, 1463

47. Kunz M. W., Schekochihin A. A., Chen C. H. K., Abel I. G., Cowley S. C. Inertial-range kinetic turbulence in pressure-anisotropic astrophysical plasmas. J. Pl. Ph., 2015, 81, 325810501.

48. Southwood D.J., Kivelson M.G. Mirror instability: 1. Physical mechanism of linear instability. J. Geophys.Res., 1993, 98, 9181-9187.

49. Kivelson M.G., Southwood D.J. Mirror instability II. The mechanism of nonlinear saturation. J. Geophys. Res., 1996, 101, 17365.

50. Matteini L., Hellinger P., Landi S., Trávnícek P., Velli M. Ion Kinetics in the Solar Wind: Coupling Global Expansion to Local Microphysics. SSRv, 2012, 172, 373.

51. Gary S.P. Short-wavelength plasma turbulence and temperature anisotropy instabilities: recent computational progress. RSPTA, 2015, 373, 40149.

52. Kennel C.F., Petschek H.E. Limit on stably trapped particle fluxes. J. Geophys.Res., 1966, 71, 1.

53. Scharer J.E., Trivelpiece A.W. Cyclotron wave instabilities in a plasma. Physics of Fluids, 1967, 10, 591

54. Gary S.P., Karimabadi H. Linear theory of electron temperature anisotropy instabilities: Whistler, mirror, and weibel. J. Geophys.Res., 2006, 111, A11224.

55. Hollweg J.V., V'olkH. J. New plasma instabilities in the solar wind. J. Geophys.Res., 1970,75, 5297, DOI: 10.1029/JA075i028p05297.

56. Marsch L., Zhao E., Tu C.-Y. Limits on the core temperature anisotropy of solar wind protons. Ann. Geophys., 2006, 24, 2057-2063.

57. Gary S.P., McKean M. E., Winske D., Anderson B.J., Denton R. E., Fuselier S.A. The proton cyclotron instability and the anisotropy beta-inverse correlation. J. Geophys. Res., 1994, 99, 5903-5914.

58. Pokhotelov O.A., Sagdeev R.Z., Balikhin M.A., Treumann R.A. Mirror instability at finite ion-larmor radius wavelengths. J.Geophys. Res., 2004, 109, A09213, DOI: 10.1029/2004JA010568.

59. Hasegawa A. Drift mirror instability in the magnetosphere. Physics of Fluids, 1969, 12, 2642.

60. Quest K.B., Shapiro V.D. Evolution of the fire-hose instability: Linear theory and wave-wave coupling. J. Geophys. Res., 1996, 101, 24457-24469.

61. Hellinger P., Matsumoto H. New kinetic instability: Oblique Alfvén fire hose, J. Geophys. Res., 2000, 105, 10519-10526.

62. Treumann R.A., Baumjohann W. Advanced space plasma physics. London: Imperial College Press, 1997.

63. Gary S.P. The mirror and ion cyclotron anisotropy instabilities. J. Geophys.Res., 1992, 97, 8519-8529.

64. Kaufmann R. L., Horng J. T., Wolfe A. Large amplitude hydromagnetic waves in the inner magnetosheath. J. Geophys. Res., 1970, 75, 4676.

65. Winterhalter M., Neugebauer B.E., Goldstein E.J., Smith S.J., Bame S., Balogh A. Ulysses field and plasma observations of magnetic holes in the solar wind and their relation to mirror mode structures. J. Geophys. Res., 1994, 99, 23371-23381.

66. Russell C.T., Riedler W. Mirror instability in the magnetosphere of comet Halley. Geophys. Res. Letters, 1987, 14, 644-647.

67. Erdos G., Balogh A. Statistical properties of mirror mode structures observed by Ulysses in the magnetosheath of Jupiter. J. Geophys. Res., 1996, 101, 1-12.

68. Cattaneo M.B., Basile C., Moreno G. Evolution of mirror structures in the magnetosheath of saturn from the bow shock to the magnetopause. J. Geophys. Res., 1998, 103, 11961-11972.

69. Burlaga L.F., Ness N.F., Acna M.H. Trains of magnetic holes and magnetic humps in the heliosheath. Geophys. Res. Letters, 2006, 33, L21106, DOI:10.1029/2006GL027276.

70. Price C.P., Swift D.W., Lee L.C. Numerical simulation of nonoscillatory mirror waves at the earth's magnetosheath. J.Geophys. Res., 1986, 91, 101-112.

71. Kasper J.C., Lazarus A.J., Gary S.P. Wind/SWE observations of firehose constraint on solar wind proton temperature anisotropy. Geophys. Res. Lett., 2002, 29, 1839,

72. Maruca B.A., Kasper J.C., Bale S.D. What Are the Relative Roles of Heating and Cooling in Generating Solar Wind Temperature Anisotropies? Ph. Rv. L., 2011, 107,

73. Maruca B.A., Kasper J.C., Gary S.P. Instability-driven limits on helium temperature anisotropy in the solar wind: observations and linear Vlasov analysis. Ap. J., 2012, 748, 137.

74. Bourouaine S., Verscharen D., Chandran B.D.G., et al. Limits on alpha particle temperature anisotropy and differential flow from kinetic instabilities: solar wind observations. Ap. J. L., 2013, 777, L3.

75. Vedenov A.A., VelikhovE.P., Sagdeev R.Z. Special Issue: Stability of Plasma. SvPhU, 1961, 4, 332.

76. Davidson R.C., V'olk H.J. Macroscopic Quasilinear Theory of the GardenHoseInstability, Ph.Fl., 1968, 11, 2259.

77. Kennel C.F., Petschek H.E. Limit on stably trapped particle fluxes. J.Geophys.Res., 1966, 71, 1.

78. Gary S.P., Feldman W.C. A second order theory fork||B0electromagnetic instabilities. Ph. Fl., 1978, 21, 72.

79. Yoon P.H., Wu C., de Assis A.S. Effect of finite ion gyro-radius on the fire-hose instability in a high beta plasma. Ph. Fl. B., 1993, 5, 1971.

80. Paesold G., Benz, A. O. Test particle simulation of the Electron Firehose instability. Astron.Astrophys., 2003, 401, 711.

81. Camporeale E., Burgess D. Electron firehose instability: Kinetic linear theory and 2D particle-in-cell simulations. J. Geophys.Res., 2008, 113, A07107.

82. Hau L.-N., Wang B.-J. On MHD waves, fire-hose and mirror instabilities in anisotropic Plasmas. Nonlin. Processes Geophys., 2007, 14, 557-568. www.nonlin-processes-geophys.net/14/557/2007/.

83. Michno1 M. J., Lazar1 M., Yoon P.H., Schlickeiser R. Effects of electrons on the solar wind proton temperature anisotropy. Ap. J., 2014, 781, 49, DOI:10.1088/0004-637X/781/1/49.

84. Kennel C.F., Scarf F.L. Thermal anisotropies and electromagnetic instabilities in the solar wind. J. Geophys.Res., 1968, 73, 6149. DOI: 10.1029/JA073i019p06149

85. Lazar M., Poedts S., Schlickeiser R. Proton firehose instability in bi-Kappa distributed plasmas. Astron.Astrophys, 2011, 534, A116. DOI: 10.1051/0004-6361/201116982

86. Remya B., Reddy R.V., Tsurutani B.T., Lakhina G., Echer E. Ion temperature anisotropy instabilities in planetary magnetosheaths. J. Geophys. Res. 2013, 118, 785-793.

87. Ahmadi N., Germaschewski K., Raeder J. Effects of electron temperature anisotropy on proton mirror instability evolution, arXiv:1602.03411v1 [physics.plasm-ph] 2016.

88. Pokhotelov O.A., Balikhin M.A., Alleyne H.St-C.K., Onishchenko O.G.Mirror instability with finite electron temperature effects.J.Geophys .Res., 2000, 105, 2393.DOI:10.1029/1999JA900351.

89. Kuznetsov E.A., Passot T., Sulem P.L. On the mirror instability in the presence of electron temperature anisotropy. Physics of plasmas, 2012, 19, 090701.

90. Matteini L., Hellinger P., Schwartz S.J., Landi S. Fire hose instability driven by alpha particle temperature anisotropy. Ap. J., 2015, 812, 13.

91. Sharma P., Hammett G. W., Quataert E., Stone J. M. Shearing Box Simulations of the MRI in a Collisionless Plasma. Ap. J., 2006, 637, 952.

92. Kunz M.W., Schekochihin A.A., Stone J.M. Firehose and Mirror Instabilities in a Collisionless Shearing Plasma. Ph. Rv. L., 2014, 112, 205003.

93. Riquelme M.A., Quataert E., Verscharen D. Particle-in-cell Simulations of Continuously Driven Mirror and Ion Cyclotron Instabilities in High Beta Astrophysical and Heliospheric Plasmas. Ap. J., 2015, 800, 27.

94. Sironi L., Narayan R. Electron Heating by the Ion Cyclotron Instability in Collisionless Accretion Flows. I. Compression-Driven Instabilities and the Electron Heating Mechanism. Ap. J., 2015, 800, 88.

95. Schekochihin A.A., Cowley S.C., Kulsrud R.M., Hammett G.W., Sharma P. Plasma Instabilities and Magnetic Field Growth in Clusters of Galaxies. Ap. J., 2005, 629, 139.

96. Mogavero F., Schekochihin A.A. Models of magnetic field evolution and effective viscosity in weakly collisional extragalactic plasmas. MNRAS, 2014, 440, 3226.

97. Drake J.F., Opher M., Swisdak M., Chamoun J.N. A magnetic reconnection mechanism for the generation of anomalous cosmic rays. Ap. J., 2010, 709, 963.

98. Schoeffler K.M., Drake J.F., Swisdak M. Scaling of the Growth Rate of Magnetic Islands in the Heliosheath Ap. J. L., 2012, 750, L30.

99. Matteini L., Landi S., Velli M., Matthaeus W. H. Proton Temperature Anisotropy and Magnetic Reconnection in the Solar Wind: Effects of Kinetic Instabilities on Current Sheet Stability. Ap. J., 2013, 763, 142.

100. Gingell P.W., Burgess D., Matteini L. The Three-dimensional Evolution of Ion-scale Current Sheets: Tearing and Drift-kink Instabilities in the Presence of Proton Temperature Anisotropy. Ap. J., 2015, 802, 4.

101. Oraevskii V.N., Konikov Y.V., Chazanov G.V. Transport processes in anisotropic near-Earth plasma. Nauka, Moscow, 1985, 173 p.

102. Ramos J.J. Dynamic evolution of the heat fluxes in a collisionless magnetized plasma. Phys. Plasmas, 2003, 10, 3601.

103. Dzhalilov N.S., Kuznetsov V.D., Staude J. Wave instabilities of a collisionless plasma in fluid approximation. Contrib. Plasma Phys., 2011, 51, No. 7, 621-638.

104. Dzhalilov N.S., Kuznetsov V.D. Low_Frequency Instabilities of Collisionless Plasma and the 16-Moment Approximation. Plasma Physics Reports, 2013, 39, No. 12, 1007-1015.

105. Hall A.N. Finite ion Larmor radius modifications to the firehose and mirror instabilities. J. Plasma Physics, 1979, 21, 431-443.

106. Kuznetsov V.D., Dzhalilov N.S. MHD Instabilities of Collisionless Space Plasma with Heat Fluxes. Geomagnetism and Aeronomy, 2014, 54, No. 7, 886-891.

107. Dzhalilov N.S., Kuznetsov V.D., Staude J. Wave instabilities in anisotropic magnetized space plasma. Astron. Astrophys., 2008, 489, 769-773.

GÜNƏŞ KÜLƏYİ FİZİKASINDA BİR PROBLEM

N. S. Cəlilov

N.Tusi adına Şamaxı Astrofizika Rəsədxanası,
Azərbaycan Milli Elmlər Akademiyası, Şamaxı rayonu, Azərbaycan

Son illər Günəş küləyi plazmasında temperatur anizotropluğunun xüsusiyyətlərinə aydınlıq gətirmək üçün intensiv tədqiqatlar aparılmışdır. Günəşdən müxtəlif məsafələrdə Günəş küləyi parametrlərinin bir sıra peyk ölçmələrinin nəticələri onu göstərmişdir ki, temperatur anizotropluq dərəcəsinin paylanması xüsusi formaya malikdir. Lakin bu paylanmanın bütün aspektləri başa düşülən deyil və nəzəri modelləşdirilməsi mümkün olmur. Bu məqalədə bu problemin həlli istiqamətində əldə olunan nəticələrin əks olunduğu qısa ədəbiyyat icmalı verilmişdir.

Açar sözlər: Günəş küləyi plazması – Temperatur anizotropluğu – Heliosfer

MAGNETIC FIELDS AND ACTIVITY OF YOUNG STARS

N. Z. Ismayilov*

Shamakhy Astrophysical Observatory named after N.Tusi,
Azerbaijan National Academy of Sciences, Shamakhy region, Azerbaijan

The magnetic field is the veryimportant factorfor the interpretation of many observed physical properties of T Tauri and Herbig Ae/Be type young stars.This review presents the state of the problem of studying selected types of young stars in the context of magnetic fields and its manifestation in the activity of these stars.

Keywords: Pre-Main Sequence stars – Spectral and photometric activity – Magnetic fields.

INTRODUCTION

One of the fundamental problems of modern stellar astrophysics is the study of the early stage of stellar evolution and the starformation processes. This is necessary for interpretation of the observational characteristics of the stars in the early stages of their evolution, for testing whether is possible to describe these characteristics with the modern theory of stellar evolution and for toimproving and developing of the theory of formation of stars and planets.Despite the fact that more than half a century of intensive researches havebeen allowed us to accumulate the immense information on the characteristics of individual groups of young stars, by now our knowledge on the early stage of stars evolution are remaining rather scarce.

The urgency of studying the early stage of evolution of small and intermediate mass stars is due to the fact that: a) these stars are the first optical radiation sources after their immediately formation as stars in the regions of starformation of the Galaxy from the interstellar gas-dust clouds; b) these stars are the precursors of our solar system and represent interest in studying theformation of planets in the early stages of evolution. Therefore, to study of such objects makes possible

* E-mail: ismailovn@yahoo.com

to understand their physical conditions in the initial stage of evolution, and also in general, would be help to solve the most important problems of starformation. Despite the fact that more than half a century has passed since the discovery of young stellar aggregates, where the formation of stars and the very early stage of their evolution still now are observed, many questions of modern astrophysics connected with this stage of stellar evolution are still incomplete.

The most important key for understanding the early stage of stellar evolution is the study of T Tauri (TTS) and Ae/Be Herbig (HAeBe) stars. These stars we know as the first formations,which are just "born" from gas-dust mother clouds of starformationof the young stars. These types of stars differ only in their physical parameters (the mass and luminosity of TTS are in range $0.5-2M_{\odot}$ and $1-5L_{\odot}$, and in the HAeBe stars, $2-10M_{\odot}$ and $50-100L_{\odot}$, respectively), and in many observational characteristics they are demonstrating a large similarity.

By now, it has become known that a magnetic field plays a key role in explaining the many physical properties of young stars. This review presents the state of the problem of studying selected types of the young stars in the context of the magnetic fields and its influenceon the activity of such stars.

1. GENERAL CHARACTERISTICS OF YOUNG STARS

1.1. TTauri-type stars

The T Tauri type Stars (TTS) were first discovered by Joy [74,75] as the irregular variables in dark gas-dust regions that show strong radiation in the emission lines H and K CaII, as well as in the Balmer series hydrogen lines and in some metal lines. Prior to this time, these stars were known as the irregular variables associated with the dark clouds and reflective nebula. The spectral classes of these stars are taking in the interval F-M, but mainly G-K and the types of luminosity IV-V.

The first systematic studies of TTS were performed by Herbig [49–51]. The main proofs of the youth of these stars are:

a) *Location in association with the regions of star formation;* the starformation regions are characterized by a combination of nebulae, OB associations and a group of infrared objects. TTSco-existwith these objects and often is forming so-called T-associations or entered to the O-association [95].

b) *Location on the Hertzsprung-Russell diagram (HR);* In HR diagram the TTS are located up to the Main Sequence (MS), where as a rule,placed late type stars.The TTS are in the stage of gravitational contraction [23,80], shows a satisfactoryagreementof the physical parameters, predicted intheoretical models for Pre-main sequence (PMS) stars.

c) *spectral characteristics;* The strong activity of stars [50,51,64,65,103] as a result of which are formed variable emission lines, which indicates the existence of a developed accretion disk or stellar wind. The strong absorption line Li λ 6707 Å in the spectrum is showing an unusual high abundance of lithium, which is also probably is indicator of the youth of TTS.

The first detailed research results of TTS [50] was published in 1962 and contains a list of 136 stars with data on star brightness, type of variability, and on intensity of strong emission lines. Later, the most complete catalogue of young stars was presented by Herbig and Bell [52]. There are several proposed genetic common subclasses of TTSs:

1) CTTS (Classical TTS) -have spectra later on K0 and the strong emission line Hα (W (Hα) $\geq$ 10 Å) [53].

2) WTTS (weak-line TTS) -TTS with weak emission in the line Hα, (W (Hα) $<$ 10 Å), the spectrum is usually later than K0. CTTS and WTTS are usually well distinguished from each other on the level of development of the emission line spectrum [53–56].

3) NTTS (naked TTS) - the evolved TTS stars, which in the course of evolution was lost the circumstellar disk and envelope surroundedof the star [116,117].

4) ETTS (early-type TTS) is a TTS with a spectrum earlier than K0, the spectral variability differs in a certain way from CTTS [53].

5) PTTS (Post TTS) stars before entering the line of the MS, this group is not so clearly differed from type NTTS [94].

Among the CTTS, the subgroup of YY Orion stars is distinguished, in which the spectral lines sometimes are showing the inverse P Cyg profile [115], and sometimes alternating red and blue shifts of the absorption components [79]. This indicates the existence of the same star the rejection and falling of matter in the atmosphere.

As noted above, TTS are low-mass stars with an age of several million years, at the stage of gravitational contraction to the MS. In subgroup of CTTS, thematter accretion from the circumstellar disk was observed [39,96]. Understanding of the accretion processes in CTTS is one of the main tasks for evolution of stars to the MS. In fact, accretion is a long-term process for the formation of mass and angular momentum of stars. Evolution and the gradual weakening of circumstellar accretion disks is an important direction in the discovery of extrasolar planets and planetary systems with unknown new properties. Therefore, the acquisition of new properties of young stellar systems, their discs and the mass loss by stellar wind is an important step towards establishing plausible scenarios for the formation of stars and planets.

1.2. The HAeBe type stars

As was noted in theintroduction, the Ae/Be Herbig type stars (HAeBe) are more massive members of young PMS stars. These stars often are called HES or HAeBe stars. About this group (for 26 stars) the following characteristics were determined first time in the classical work of Herbig [48] in 1960:

1. Spectral classes in range B-A, strong emission lines of hydrogen.
2. The stars are in the dark nebula.
3. The stars are illuminatedthe nebula in their immediate vicinity.

These properties distinguish the HAeBe stars from the classical Be stars of the same spectral types. Later it was found out that many of properties of HAeBe stars are analogous to the properties of TTS stars [6, 7, 28, 78, 110]:

a) There is an infrared (IR) excess of radiation in many HAeBe stars, and this indicates the existence of the dust envelope around the star.

b) Irregular variability of light and spectrum. The variability of profiles and the intensity of the emission lines were observed [102].

c) Linear polarization of the radiation is about 1% in the continuum; in some HAeBe stars, the polarization reaches 7-8%, which distinguishes them from the classical Be stars.

d) All these stars are located in gas-dust star formation complexes. All these properties show that HAeBe type stars are at the initial stage of evolution and are stars with intermediate masses between OB stars and TTS.

2. SURFACE ACTIVITY

A common property of the emission spectra of young stars is the irregular variability of the intensities and line profiles on the time scale from weeks and months to days [53, 61, 98]. However, long-term observational data make it possible to detect periodic or quasi-periodic variations in brightness and spectrum [37, 62, 99, 100]. Some stars in decades of systematic observations show cyclic changes in brightness over 6-10 years [63].

Irregular variability in brightness is characteristic of most CTTS, while many WTTS show periodic light changes [29]. The most complete catalog of UBVR observations of the large number of TTS and HAeBes is given in the works of Herbst et al. [53, 55]. According to the results of analysis of the large number of observations, we can now distinguish three basic physical mechanisms of TTS variability, in which the magnetic field plays a dominant role:

1) Rotational modulation of the star's brightness with cool spots on the surface. This is a periodic variability with a range of periodsfrom 2 to 12 days and

amplitude of several hundredths to a few tenths of the magnitude. This event was observed mainly in WTTS. A typical example is the V410 Tau [47,97,107].

2) Variable rate of gas accretion on the surface of the star, short-lived hot spots on the surface. Irregular or quasi-periodic brightness variations with amplitude of up to 1-3 mag, with a characteristic time of several days. It is observed only in CTTS. A typical example: BP Tau [42].

3) Variable basically, circumstellar extinction on the line of sight, i.e. the eclipse of the star by gas-dust clouds. Irregular light fades with amplitude 2-3 mag is observed, mainly, in CTTS. The WTTS no longer have dust accretion disks near the star, the inner regions of the disk have already dissipated, so there is no circumstellar dust that could eclipse the star. Although, in principle, there may be a case where WTTS is observed exactly in the plane of the residual disk and the star can be eclipsed by far parts of the disk. Irregular light fades in the most explicit form is observed in young stars of an earlier spectral class (Ae/Be Herbig star, such as UX Ori) [55, 105]. It is characteristic that when the brightness is weakened, the color-index first increases (reddened), and then decreases (became blue): as the star is eclipsed, the contribution of light scattered on the dust particles is increased [102]. In the deep minima of light, linear polarization is increased. The spectrum does not change even with significant decrease in light. A typical example: RY Tau [66, 98].

The surface activity of TTS can be observed in the form of the short-term change in brightness and spectrum [97], which can be divided into two types: rapid changes, less than about 1 day, and slow changes occurring within 2-8 days. For rapid changes Gahm et al. were [29] discovered two different types of events for six stars (CTTSs two, three WTTSs, and one PTTS) characterized as follows:

a) Flares in the Balmer lines and in the continuum - a rapid increasing a radationin the Balmer continuum and in the hydrogen emission lines of the Balmer series for a time interval of less than 1 hour. This type of event is occured only in WTTS. For explaining of this eventGahmet al. [29] assumed that the flareis occured on the surface of the star, since is due to dissipation of the magnetic field energy. Although the detailed mechanism of such event is unknown, the observed flares are extremely powerful ($10^{33} - 10^{34}$ ergs) relatively with the flares which are occured in ordinary flare stars.

b) Increasing the continuum - a slow and smooth increase in the continuum level after several hours. It is assumed that its origin is due to the accretion of the inhomogeneous matter from the circumstellar disk.

Slow changes during 2-8 days are explained by surface activity and modulation of brightness by rotation of the star. Bouvier and Bertout [9] have founded periodic variations in 15 TTS. The value of periods is in the range of 1.9-8.5 days. Most likely, there are dark spots on the surface of these stars [31,89], which have

a temperature 500 - 1000 K below than the photosphere and they are occupied up to 3-17% areas of the photosphere surface.

Also stars with hot spots are observed, although the number of such stars is small. Such spots should be hotter than photospheres - up to 7000 K, but their coverage areas are generally less than 1%. Bouwier and Appenzeller [10] suggested that hot spots were arisen as a result of the accretion of matter flows from the circumstellar disk and as a result of the formation of the shock front on the surface of the star.

The surface activity of young stars is directly related to magnetic fields [31, 41, 43, 60, 90]. While the existence of strong magnetic fields for TTS stars up to 1 KGs and more has already been observed several times [20, 70, 73, 120], studies on the direction of detection of such magnetic fields in HES type stars are very small [56], but now intensive research is being done in this direction.

Relatively well in recent years, the characteristics of the magnetic field in CTTS have been studied (see [72] and references cited therein). The strength of the magnetic field averaged over the surface are several kGs. These fields are responsible for several processes in CTTS - a) X-ray radiation from the stellar corona with the influence of the magnetic field, b) keep of the circumstellar disk at the distance of several star radii and c) control of the magnetospheric accretion process.

In studying of these processes, in addition to the average value of the magnetic field, it is necessary to know the topology of large-scale magnetic fields on the stellar surface. These studies were performed by using the Zeeman-Doppler imaging technique (Zeeman-Doppler Imaging-ZDI). On the basis of this method is lied a spectropolarimetric observations of stars for several rotation periods with a high time resolution and the restoration of the distribution and orientation of a large-scale magnetic field on the surface of the star [24–27]. In these papers it was shown that the topology of the magnetic field in different TTS often is symmetric as for example in both AA Tau and BP Tau, but also has a more complex structure in some individual stars.

3. THE MAGNETOSPHERIC ACCRETION MODELS AND THE LINE PROFILES

The concept of the disk accretion, applied to a wide range of astrophysical objects, is based on the theoretical papers [104] and [83]. The matter of the accretion process, controlled by the magnetic field was used in many compact objects. This model seems very fruitful in explaining the star formation in low mass objects, and is also used for explaining the accretion of matter in white dwarfs (AM Her) [118], accretion in pulsars or X-ray sources [112], and accretion to black holes in

the active galaxy nucleus [5,19]. The assumption on the existence of strong magnetic fields on the surface of TTS is based on their strong radiation in the X-ray and centimeter radio ranges [1,87]. Magnetic fields of the order of 1-3 kGs were measured on the Zeeman widening of photospheric lines in CTTS [40,67,68], as well as in maser cyclotron radiation [108]. It is assumed that these strong stellar magnetic fields substantially changes the accretion and outflow fluxes in the circumstellar disk near the central star.On the interaction of the circumstellar disk and magnetic fields in TTS is given in the book is published on the materials of the IAUsymposium [11].

The conception of the magnetically controlled accretion in CTTS was developed in the 1980s. By using model [32] applied to X-ray pulsars, in works [15] and [77] were used a dipole magnetic field that which is formed a magnetosphere and is extended over several stellar radii, where the rate of accretion to the surface of the star is $10^{-9} - 10^{-7} M_{\odot}$ year $^{-1}$. At a typical magnetic field strength in TTS, and at the typical accretion rate, the equality of the magnetic pressure and the dynamic pressure of the moving substance occurs at the distance of several radii from the star. Under these assumptions on the existence of such equilibrium, in works [16, 77, 106] an analytical expression was obtained for the strength of the dipole magnetic field of the star as a function of the parameters of the star and its accretion disk. Closer to the star, the magnetic field is completely controlled the movement of the gas. The gas temperature on the surface of the staris increased sharply in the wave shock. The radius of corotation is the distance from the star, where the angular velocity of the star is equal to the angular Keplerian velocity. At this distance, the substance is rotating in the disk moves with the same velocity as the magnetic-sphere of the star. For TTS this distance is equal to the several stellar radii. As a result of the evolution of the star's angular momentum, the inner boundary layers of the accretion disk (where wasestablished the equality ofmagnetic and dynamic pressures) is established near the corotation radius.

Nowadays many various similar models have been proposed and are applied to the phenomena of TTS. For to studying the formation of profiles of emission lines, Muzerolle et al. [89] have presented a model with the dipole magnetic field and an axisymmetric accretion flow. In this case, the external and internal parameters of the disk are taken as free parameters. Solving the equation of radiation transfer, they calculated the profiles of the lines Hα, Hβ, D NaI, the parameters of the accretion rate, the gas temperature, the disk inclination angle and the size of the magnetosphere. The model also allows to carry out diagnostics on emission lines, by changing the parameters which are forming the line profile. In the work [90], this model was applied to the data of Ae/Be Herbig type star UX Ori, and acceptable disk parameters were obtained.

In favor of the accretion modelthere are such observational facts as the veiling of the absorption spectrum due to the continuum emission, as well as the signs of the higher temperature on the surface of the star, relatively with the rest of the photosphere [3, 41, 43, 113]. In the interpretations it was assumed that the stellar magnetic field of the star most likely is stopped disc accretion at the certain distance from the star and at large latitudes the circumstellar matter accretion is occurs on the star's surface in the form of jets along the magnetic force lines ("tubes") [4, 92, 106]. When the matter from the accretion disk is reaches to the surface of the starit is formed a shock front and generated an optical excess of radiation. Such events were observed in the CTTS. Recently, has been developed the theoretical work on the structure of accretionary impact in the magnetic-spherical accretion model [81,82], which makes it possible to calculate the excessin the continuum and in the linear spectrum of CTTS. In [14]was performed a detailed calculation of the accretion shock structure in CTTS, the results of which agrees well with the observations. A satisfactory agreement was also obtained on the calculated emission line intensities in the UV part of the spectrum with observations in CTTS [33,34]. On the other hand, it is known that CTTS possess strong magnetic fields and from systematic observations of IUE, emission in TTS can be occur by both factors – becauseof magnetic and accretion processes.

According to [56–59], the intensity of the magnetic field in HAeBe stars should not be less than 100 G, and for one of the typical HAeBe stars AB Aur, according to [17], it reaches 1 kG. In the existing subgroup of HAeBe stars the type UX Ori (stars whose non-periodic light fading is observed in range at 2-3 mag), which possess the observed stellar wind at the order $3 \cdot 10^{-7} M_{\odot}$ year^{-1}, for to accordance with the accretion model requires a magnetic field of the order of 560 G [109]. For the UX Ori type stars, an alternative model has also been developed, where is explaining the weakening of the star's brightness by screening its surface with comet-like bodies around the star [109].

Observational and theoretical studies of the gas-dust disk around the young stars, in particular, lead to the idea that the disk accretion provides excess radiation [45,46]. Theoretical estimates of the disk parameters and the radiation of the underlying layers in the continuum is satisfactory agreed very well with observations, although these models do not take into account the physical environment of the star [4, 69, 76].

Even is more incomprehensible the structure of the outer disk and the underlying layers, where emission lines are presumably formed. The observed correlation in TTS between the IR excess and some standard indicators of the stellar wind (for example, the profiles of Hα and forbidden lines) show that the disk accretion in TTS controls the flow of matter [2,13]. But the mechanisms of this interaction are still unclear.

The concept of the spatial structure of the region where the emission lines of HAeBe and TTS stars are formed is also ambiguous. Although in recent years there have been obtained some results in this direction [44,46,71,84], the available data are still insufficient and further studies are required.

The accretion of the substance in CTTS seems to cause an accretion shock, which is resulting an additional ultraviolet (UV) emission. It was observed a correlation with the increase in luminosity and in intensitiesof some emission lines. For the classical TTS by the age of about 1 million years, the mass accretionrate increases by 1-2 orders, which is allowing to estimate of the time of dissipation of the outer gas-dust shell. Measurements of the dust radiation in the long-wave part of the spectrum make it possible to estimate the mass of the disk and the point of dissipation of the inner regions of the disk [21]. In so-called transit disks, where the IR radiation at $\lambda \geq 10\,\mu m$ is very weak, the energy distribution in the spectrum is interpreted as a short stage of disk evolution between the optically thick phase and the optically thin scattered disk [22, 119]. At this stage can be arises Jupiter like planets [91].

As noted above, HAeBe stars are more massive objects, have intermediate masses between TTS and stars with M$\geq$10 $M_{\odot}$. Apparently, these stars, like TTS, can be detected as soon as they are started the radiation in the optical range. These extremely interesting objects must evolve faster than the TTS, and consequently, the planet formation processes must be going faster [8, 12]. The observed number of HAeBestars is smaller than that of TTS, which is the result of the higher rate of their evolution. The spectral classes may be in the interval O9 - F2, and these stars are surrounded by the residual gas-dust disk, which, as a result of the thermal radiation of the circumstellar disk, is formed an IR excess in the spectral continuum. Direct images of disks for several stars were obtained from IR observations [36]. The circumstellar disks of HAeBe type stars have a complex structure. At the equatorial part of star the matter accretion comes from the inner part of the disk (in the equatorial plane), while at high latitudes, there is an outflow (wind). On the other hand, the disk wind can betransferedof the excess angular momentum [30]. Indicators of the circumstellar disk in the spectrum can give information on the interaction of the central star with the disk. The interaction of the central star and the circumstellar disk has been studied quite well for low mass MS stars. For example, the TTS have a dipole magnetic field of the order of several kG. The interaction of the disk-star system in TTS stars is described within the framework of the magnetospheric accretion (MA) model [11]. According to the model MA, the pressure created by the accretion substance from the disk at a certain distance from the star is balanced by the pressure created by the stellar magnetic field.On this radius of collision, the accreting substance is guided along the magnetic force lines and with the ballistic velocity it falls to the

stellar surface.

This situation is not quite clear for the case of HAeBe type stars. In the inner parts of such stars are thermal rays dominated by radiant radiation transfer [59]. However, for the formation of the strong magnetic field bythe dynamo mechanism, it is requiredthe convection. Nevertheless, it is likely that most late-type HAeBe stars, with the spectrum later than B9 (HAe), as a result of evolution, arose from TTS intermediate masses with K-G spectra which have subatmospheric convective zones, where magnetic fields are formed [93]. In addition, it is likely that the magnetic field of HAeBe type stars can arise as a result of differential rotation of the star or as the result of appearance the dynamo mechanism in the circumstellar disk [111]. Recent direct measurements of the magnetic field by the spectro-polarimetrymethod have made it possible to reveal longitudinal magnetic fields in some HAe stars of the order of several hundred Gauss [57–59, 114]. As shown in [35, 88, 90], the disk accretion existing in HAe stars controlled by the magnetic field is occurred through magnetic tubes. In any case, in HAe stars with the magnetic field of about 100 G, the magnetosphere radius relatively to the TTS stars should be much smaller. As a result, we must obtain the character of disk-star interaction in HAe stars different from TTS.

Recently 56 HAeBe type stars were studied in the IR range spectrum at the line HeI 10830 [18]. The authors found a significant difference in the HAeBe for blue- and red-shifted absorption components (flow and fall of matter) from CTTS. It is shown that unlike CTTS, HAeBe does not accrete from the internal disk. This indicates a significant difference in the structure of the magnetosphere of these stars.

According to [38], in principle, the magnetospheric accretion scheme is applicable to the HAeBestars, with the only difference being that these stars do not possess such a strong magnetic field as T Tauri type stars, and do not have a developed magnetosphere. For most rapidly rotating stars the magnetosphere of HAeBestars occupies an area of the order 2-3 star radii whereas in T Tauri type stars it extends to 5-10 stellar radii.

The accretion activity of HAeBe stars can't be considered separately from the outflow of matter, without which accretion into the star itself would be impossible [38]. In addition, the accretion and outflow of matter in young stars are closely connected to the magnetic field of the disk and/or the stars, the origin and configuration of which at this moment are the subject of discussions.

Recently, in [101] by using photometric data, the light curves of well-known T Tauri stars are analyzed. The authors analyzed 7-year light curves and showed that 4 stars from the group have periodic variability with periods of 20-60 days. Such variability is stably and can be observed from month to year. It was ex-

plained by the interaction of the circumstellar disk and the magnetic field of the star.

As indicated above, the existence of the global magnetic field of several kG in CTTSs can be considered as a proven fact [24, 70]. Such magnetic field is approximately several thousand times stronger than the global magnetic field of the Sun. The results of observations shows that most TTSsare rotating more slowly, about 10% lower than expected [54]. This is unexpected, because as a result of disk accretion, the angular momentum should be increased. Further studies have shown that the existence of a significant magnetic field can affect the dynamics of the circumstellar environment. The field promotes rupture of the disk and the accretion of matter along the magnetic field lines to the surface of the star. This gives rise to an accelerating mechanism for various kinds of outflows, including wind along open magnetospheric lines [85, 86]. In these papers several problems are discussed, according to the scenario of disk outflow, where it was shown that the topology of the stellar magnetic field should be open. The existence of open field magnetic lines contributes to the appearance of the stellar wind, which could transfer a significant angular momentum. Calculations showed that the loss of angular momentum from such a wind is about 10% of the original value [85].

4. CONCLUSIONS

In the above presented brief review, various forms of activity of young stars and methods of their interpretation with allowance of the magnetic field of the star are described. Unfortunately, at this moment there are no reliable observational data that would be allow to studying variations in the spectrum and/or brightness of the star in parallel with measurements of the magnetic field in individual young stars. Such observational data can be obtained from observations of the group of known magnetic stars, and in young stars with a large value of the magnetic field, as well as in the group of young stars that do not have information on the magnetic field, but the star is physically highly active. Carrying out the correlation analysis between different spectral, photometric and spectropolarimetric parameters of individual stars, and by using modern methods, would be make it possible to clarify the structure of the magnetic field and its role in the activity of young stars.

REFERENCES

1. André P., 1987, CEA, France, 143

2. Basri G., Bertout C., 1989, Astrophys.J., 341, 340

3. Bastian U., Finkenzeller U., Jascheck C., Jascheck M., 1983, Astron. Astrophys., 126, 438

4. Bertout C., Basri G., Bouvier J., 1988, Astrophys.J., 330, 350

5. Bisnovatyi-Kogan G. S., Giovannelli F., 2017, Astron.Astrophys., 599, A55

6. Bohm T., Catala C., 1994, Astron.Astrophys., 290, 167

7. Bohm T., Catala C., 1995, Astron.Astrophys., 301, 155

8. Boss A. P., 2011, Astrophys.J., 731, 74

9. Bouvier J., Bertout C., 1989, Astron.Astrophys. 211, 99

10. Bouvier J., Appenzeller I. ed., 2007, Cambridge University Press, 375

11. Bouvier, J., Alencar, S. H. P., Harries, T. J., et al., 2007, Univ. Arizona Press., 479

12. Bowler, B. P., Johnson, J. A., Marcy, G. W., et al., 2010, Astrophys.J., 709, 396

13. Cabrit S., Edwards S., Strom S. E., Strom K. M., 1990, Astrophys. J., 354, 687

14. Calvet N., Gullbring E., 1998, Astrophys.J., 509, 802

15. Camenzind M., 1990, Rev. Mex. Astron. Astropfis., 3, 234

16. Cameron A.C., Campbell C.G., 1993, Astron. and Astrophys., 274, 309

17. Catala C., Bohm T., Donati J.F., Semel M., 1993, Astron.Astrophys., 278

18. Cauley P. W., Johns-Krull, C. M., 2014, Astrophys.J., 797, 112

19. Cherepashchuk A. M., 2017, Astron.Reports, 61, 265

20. Chuntonov G. A., Smirnov D. A., Lamzin S. A., 2007, Astron.Letters., 33, 1, 38

21. Cieza L. A.,2008, In ASP Conf. Ser. 393, 35

22. Cieza L., Padgett, D. L., Stapelfeldt, K. R., et al., 2007, Astrophys. J., 667, 308

23. Cohen M., Kuhi L. V., 1979, Astrophys. J., Suppl., 41, 743

24. Donati J.F., Jardine M. M., Gregory S. G. et al. 2007, MNRAS, 380, 1297

25. Donati J.F., Gregory, S. G., Alencar, S. H. P., et al., 2012, MNRAS, 425, 2948

26. Donati J.F., Jardine M. M., Gregory S. G. et al., 2008, MNRAS, 386, 1234

27. Donati J.F., Skelly M. B., Bouvier J. et al., 2010, MNRAS 409, 1347

28. Finkenzeller U., Mundt R., 1984, Astron. Astrophys. Suppl., 55, 109

29. Gahm G. F., Loden K., Gullbring E., Hartstein D., 1995, Astron.Astrophys., 301, 89

30. Garcia P. J. V., Ferreira J., Cabrit, S., et al., 2001, Astron.Astrophys. 377, 589

31. Gershberg R. E., Petrov P.P., 1976, Soviet Astronomy Letters., 2, 195

32. Ghosh P., Lamb F.K., 1979, Astrophys. J., 232, 259

33. Gomez de Castro A.I., Fernandez M., 1996, MNRAS., 283, 55

34. Gomez de Castro A.I., Lamzin S.A., 1999, MNRAS., 304, L.41

35. Grady C. A., Hamaguchi, K., Scheider, G., et al., 2010, Astrophys.J., 719, 1565

36. Grady C. A., Woodgate, B. F., Bowers, C. W., et al.,2005, Astrophys.J., 630, 958

37. Grankin K.N., MelnikovS.Yu., Bouvier J., et al., 2007, Astron.Astrophys., 461, 183

38. Grinin V. P. Tambovtseva L. V., 2011, Astronomy Reports., 55, 8, 704

39. Grinin, V. P., 1980, Astrophysics., 16, 2, 243

40. Guenther E. W., Lehmann H., Emerson J. P.,Staude J., 1999, Astron. Astrophys., 341, 768

41. Gullbring E., Hartmann L., Brice C., Calvet N., 1998, Astrophys.J., 492, 323

42. Gullbring, E., Barwig, H., Chen, P. S., et al., 1996, Astron.Astrophys., 307, 791

43. Hamman F., Persson S.E., 1989, Astrophys. J. 339, 1078

44. Hamman F., Persson S.E., 1992, Astrophys. J. Suppl. Ser., 82, 247

45. Hartmann L., Keyon S.J., 1990, Astrophys.J., 349, 190

46. Hatzes A.H., Kurster M., 1994, Astron. Astrophys., 285, 454

47. Hatzes A.P., 1995, Astrophys. J., 451, 784

48. Herbig G. H., 1960, Astrophys. J. Suppl., 4, 337

49. Herbig G.H., 1950, Astrophys. J., 111, 11

50. Herbig G.H., 1962, Adv. Astron. and Astrophys., 1, 47

51. Herbig G.H., 1977, Astrophys. J., 214, 747

52. Herbig G.H., Bell K.R., 1988, Lick Obs. Bull., 1111, 90

53. Herbst W., Herbst D., Grossman E. J., Weinstein D., 1994, Astron.J., 108, 1906

54. Herbst W., Eislöffel J., Mundt R. & Scholz A. 2007, in Protostars and Planets V, ed. B. Reipurth, D. Jewitt & K. Keil (Tucson, AZ: Univ. Arizona Press), 297

55. Herbst W., Shevchenko V. S., 1999, Astron.J., 118, 1043

56. Hubrig S., Schöller M., Ilyin I., et al., 2012, AIP Confer. Proceedings., 1429, 21

57. Hubrig, S., Pogodin, M. A., Yudin, R. V., et al., 2007, Astron.Astrophys., 463, 1039

58. Hubrig, S., Schöller, M., Ilyin, I., et al., 2011, Astron.Astrophys., 536, A45

59. Hubrig, S., Stelzer, B., Schöller, M., et al., 2009, Astron.Astrophys., 502, 283

60. Hussain G. A. J., 2012, Astron.Nakhr., 333, 4

61. Ismailov N. Z., Grankin K. N., 2007, Astron.Letters., 33, 113

62. Ismailov N.Z., Quliyev N.K., Khalilov O.V., Herbst W., 2010, Astron.Astrophys., 511, A.13

63. Ismailov N.Z., Samus N.N., 2003, Inform. Bull. Var. Stars., 5382, 1

64. Ismailov Z. A., 1974, Tsirk. Shemakh. Astrofiz. Obs., 35, 3

65. Ismailov Z. A., Rustamov, B. N., 1987, Soviet Astronomy Letters., 13, 51

66. Ismailov, N. Z., Shustarev, P. N.; Adigezalzade, A. N.; Bahaddinova, G. R. 2011, Astronomy Letters., 37, 11, 783

67. Johns-Krull C. M., Valenti J. A., 2001, Astrophys. J., 561, 1060

68. Johns-Krull C. M., Valenti J. A., Hatzes A. P., and Kanaan A., 1999, Astrophys.J. 510, L41

69. Johns-Krull C. M., Vatenti J. A., Linsky J. L., 2000, Astrophys. J., 539, 815

70. Johns-Krull C.M., 2007, Astrophys J. 664, 975

71. Johns-Krull C.M., Hatzes A.P., 1997, Astrophys.J., 487, 896

72. Johnstone C.P., Jardine M., Gregory S. G., et al., 2014, MNRAS 437 3202

73. Johnstone R.M., Penston M.V., 1986, MNRAS., 219, 927

74. Joy A.H., 1945, Astrophys. J., 102. 168

75. Joy A.H., 1949, Astrophys. J., 110, 424

76. Kenyon S. J., Brown D. I., Tout Ch. A., Berlind P., 1998, Astron.J. 115, 2491

77. Königle A., 1991, Astrophys. J., 370, L39

78. Kozlova, O. V., Grinin, V. P., Chuntonov, G. A. 2003, Astrophysics., 46, 265

79. Krautter J., Bastien V., 1980, Astron.Astrophys., 88, L6

80. Kuhi L. V., 1965, A short review. J. R. A. S. Canada., 60, 1

81. Lamzin S.A., 1995, Astron. Astrophys., 295, L20

82. Lamzin S.A., 1998, Astron.Reports., 42, 322

83. Lynden-Bell D., Pringle J.E., 1974, MNRAS., 168, 603

84. Mathieu R.D., Evolutionary processes in interacting binary stars 1992, IAU Symposium №151, 21M, Kluwer Academic Publishers, Dordrecht, Boston, MA.

85. Matt S., Pudritz R.E. 2008, Astrophys.J., 678, 1109

86. Matt S., Pudritz R.E. Astrophys.J., 2005, 632, L135

87. Montmerle T., Koch-Miramond L., Falgarone E., and Grindlay J. E., 1983, Astrophys.J., 269, 182

88. Mottram J. C., Vink J. S., Oudmaijer R. D., Patel M., 2007, MNRAS., 377, 1363

89. Muzerolle J., Calvet N., Hartmann L., 2001, Astrophys. J., 550, 944

90. Muzerolle, J., D'Alessio, P., Calvet, N., et al., 2004, Astrophys.J., 617, 406

91. Najita J. R., Strom S. E., Muzerolle J., 2007, MNRAS., 378, 369

92. Ostriker E. C., Shu F.H., 1995, Astrophys.J., 447, 813

93. Palla F., Stahler S. W., 1993, Astrophys.J., 418, 414

94. Pallavicini R., Pasquini L., Randich S., 1992, Astron.Astrophys., 261, 245

95. Parenago P. P., 1954, Publ. der 10. Astrometr. Konf. der UdSSR., 25, 254

96. Petrov P. P., 2003, Astrophysics., 46, 611

97. Petrov P.P., Shcerbakov V.A., BerdyuginaS.V.,et al., 1994, Astron.Astrophys. Suppl. Ser.,107, 9

98. Petrov P.P., Zajtseva G.V., EfimovYu.S. et al.,. 1999, Asrophys., 341, 553

99. Pogodin M. A., Kozlova O. V., Beskrovnaya N. G., et al., 2012, Astrophysics., 55, 480

100. Pogodin, M. A., Miroshnichenko, A. S., Bjorkman, K. S., et al., 2000, Astron.Astrophys., 359, 299

101. Rigon L., Scholz A., Anderson D., West R., 2017,MNRAS .,465,3889

102. Rostopchina, A. N.; Grinin, V. P., Shakhovskoi, D. N. et al., 2007, Astron.Reports., 51, 869

103. Salmanov I. R., 1973, Tsirk. Shemakh. Astrofiz. Obs., 1(19), 3

104. Shakura N. I., Sunyaev R. A., 1973, Astron. Astrophys., 24, 337

105. Shenavrin V. I., Rostopchina-Shakhovskaya A. N., Grinin V. P., et al., 2016, Astron.Reports., 60, 753.

106. Shu F.N., Najita J., Ostriker E., et al., 1994, Astrophys.J. 429, 781

107. Skelly M. B., Donati J.-F., Bouvier J. et al., 2010, MNRAS., 403, 159

108. Smith K., Pestalozzi M., Güdel M., et al., 2003, Astron. Astrophys., 406, 957

109. Sorelli C., Grinin V.P., Natta A., 1996, Astron.Astrophys., 309, 155

110. Strom S. E., Strom K. M., Yost J., et al., 1972, Astrophys.J. 173, 353

111. Tout C. A., Pringle J. E., 1996, MNRAS., 281, 219

112. Tutukov A. V., Cherepashchuk A. M., 1997, Astron. Reports., 41, 355

113. Valenti J.A., Basri G., Johns C.M., 1993, Astron.J., 106, 2024

114. Wade G. A., Bagnulo S., Drouin D., et al., 2007, MNRAS, 376, 1145

115. Walker M.F., 1972, Astrophys.J., 175, 89

116. Walter F. M., Brown A., Mathieu R. D., Myers P. C., Vrba F. J., 1988, Astron.J., 96, 297

117. Walter F.M., 1986, Astrophys.J., 306, 573

118. Warner B., 2004, Publ. Astron. Soc. Pac., 116, 115

119. Wolk S. J., Walter F. M., 1996, Astron.J. 111, 2066

120. Yang H., Johns-Krull C.M., 2011, Astrophys.J., 729, 83

MAQNİT SAHƏLƏRİ VƏ CAVAN ULDUZLARIN AKTİVLİYİ

N. Z. İsmayılov

N.Tusi adına Şamaxı Astrofizika Rəsədxanası,
Azərbaycan Milli Elmlər Akademiyası, Şamaxı rayonu, Azərbaycan

Cavan ulduzların bir çox fiziki xassələrini izah etmək üçün həlledici amillərdən biri maqnit sahəsidir. Təqdim olunan xülasədə maqnit sahəsi və cavan ulduzların aktivliyində onun təzahürləri kontekstində seçilmiş ulduz qruplarında problemin tədqiqat vəziyyəti şərh olunmuşdur.

Açar sözlər: Baş ardıcllıq ulduzları – Spektral və fotometrik aktivlik – Maqnit sahələri

HIGH VELOCITY ABSORPTION AND EMISSION IN THE SPECTRUM OF SUPERGIANT HD 199278

Sh. K. Ismayilova, N. Z. Ismayilov*, Kh. M. Mikailov

Shamakhy Astrophysical Observatory named after N.Tusi,
Azerbaijan National Academy of Sciences, Shamakhy region, Azerbaijan

We have presented results of spectral monitoring of the hydrogen lines Hα and Hβ for the supergiant star HD 199478 (B8Iae). We have executed a spectral monitoring for the study of the presence of unusual wide emission and high velocity absorption (HVA) phenomenon in this star which physical nature at this moment was not understood.
Our observations showed that the line profiles mainly can to be staying stable nearly during 18-24 days. Results for 4 various years of observation showed that probable is not there any strict periodic process inline profile variability (lpv). We have discovered only 22 ± 2 days more probably characteristic time of variations in the line-profile variability (lpv) of hydrogen lines. Only for one season (in 2011) during 17 days we have discovered the high velocity absorption (HVA) with the maximal displacement -510 km s^{-1}. Wide emission in the line Hα with the maximal displacement $\pm$ 500 km s^{-1} have discovered more often, than the blue absorption.

Keywords: B - supergiants – spectral variability – high-velocity outflow and accretion of matter – HD199478.

INTRODUCTION

The observed systematic variability of the stellar wind parameters by profiles and parameters of the spectral lines in bright supergiants is important for understanding the dynamics of the stellar wind and the stellar atmosphere structure. A large number of observational data obtained so far by late B and early Asupergiants (hereafter BA SGs) have shown that these stars exhibit the variability of the stellar wind in the time scale from several days to several tens of days. Completed in recent years, various observing campaigns have shown that such variability of the stellar wind is often associated with active changes which are

* E-mail: ismailovn@yahoo.com

occurring at the level of the photosphere. One of the main interesting features of these objects is the variation of the radial velocities and equivalent widths, as well as the profiles of different spectral lines in the time scale from several days to several months. For the first time, Kaufer et al. [1–3] have shown that there are only a few stars with unusually wide absorption on the blue wing of the line Hα, with a maximum displacement of up to -1200 km s^{-1} (high velocity absorption -HVA). The physical nature of the appearance of such a profile structure is still unclear. In addition, in the same stars in the line Hα, a very wide variable emission was discovered, the nature of which is not entirely clear. For a detailed study of such changes,it is necessary a long series of spectral observations with the high spectral and temporal resolution, which requires to using of large size telescopes. HD199478 (HR 8020, B8Iae, $V \approx 5.69$ mag) is the central star of the reflective nebula IC 5076. The star differs from the other B SGs in that it has an inverse radial velocity distribution for the Balmer progression - the higher members of the series have fewer displacements than the lower terms [4] and similarly to Be-stars with a double peak Hα emission [5]. For this star narrow absorption components(DACs) of the lines in the UV spectrum were detected, but their variation with time has not been studied [6]. According to Markova et al. [7] the photospheric lines have a systematic displacement relative to the star center velocity with a characteristic time of about 20 days. In addition, these authors found a significant change in the emission line Hα. According to the data of 2000, was discovered a wide absorption in the blue wing of the line, which changes for 60 days and indicated the matter accretionand outflow.

The photometric variability of the star with amplitude of 0.15 magin B and V bands was observed [8], but the reason for such changes is still unclear. In the present work new results of long-term studies of hydrogen lines Hα and Hβ in the spectrum of HD199478 are presented. The purpose of this study is execute a data analysison the long time spectral material for study a reason of an unusually wide absorption profile (HVA event) observed on the blue wing, broad emission on the blue and red wings of the line Hα, and also the time variation of the spectral line parameters in the spectrum of this star.

OBSERVATIONS AND RESULTS

Spectral observations were carried out in 2011, 2013-2015 in the Cassegrain focus of the 2-m telescopeof ShamakhyAstrophysical Observatoryof Azerbaijan National Academy of Sciences. An echelle spectrometer constructed on the base of the UAGS spectrograph was used [9]. As a light detectorwas used a CCD with 530×580 elements. Observations of the program star HD199478 were performed in the range of λ 4700-6700 Å. The description of the observational devices, the

reduction of images and processing of the material more detail were described in [9] and [10].

The spectral resolution is R = 14000. The meansignal-to-noise level in the region of the line Hα is S/N = 200-300, and in the region of the line Hβ - S/N = 100. For the reduction of wavelengths, the sky spectrum was used. The root-mean-square deviation of the points of the reference lines from the polynomial mean along the dispersion curve in different orders was $3 \cdot 106{-}2 \div 5 \cdot 10^{-2}$ mm, which in the case of positional measurements gives an error of $\pm 1.5 - 2.5$ km s^{-1}. All processing of images, their translation into a standard format and further measurement of spectrograms were performed using the DECH20T program developed at the SAO RAS [11]. The log of observations is given in Table 1, where in the columns, starting from the left to the right, are the spectrum number, the date of receipt for the middle of exposure, the time in JD, the exposition time, the S/N ratio in the region of the line Hα. Errors in the measurements of intensity due to the continuum, depending on the S/N level, were 0.5-1% in the region of the line Hα and up to 1-2% in the region of the line Hβ. The continuum level was controlled by standard stars. In this paper, we present the results of measurements and analysis on the hydrogen lines Hα and Hβ.

The following spectral parameters of the hydrogen lines Hα and Hβ were measured: equivalent widths W_λ, half-widths (FWHM), central depths and heliocentric radial velocities Vr. The mean error of measuring the line equivalent widths is not exceeding $\sim 5\%$.

Table 1. A log on the observational material

Spectrum	**Data**	**JD2455000+**	**Exposition time (sec)**	**S/N (at Hα)**
ks4024 – 25	02.07.2011	5745.399	1200	240
ks4056 – 57	04.07.2011	5747.382	1200	240
ks4077 – 78	06.07.2011	5749.396	900	140
ks4091 – 92	07.07.2011	5750.341	1200	200
ks4108 – 09	13.07.2011	5756.236	1200	140
ks4126 – 27	14.07.2011	5757.313	900	240
ks4152 – 53	19.07.2011	5762.247	900	160
ks4170 – 71	21.07.2011	5764.326	900	160
ks4197 – 98	25.07.2011	5768.414	900	150
ks4229 – 30	28.07.2011	5769.382	1200	180

Continuation of the table 1

Spectrum	**Data**	**JD2455000+**	**Exposition time (sec)**	**S/N (at Hα)**
ks4246 – 47	28.07.2011	5771.307	1200	160
ks4272 – 73	02.08.2011	5776.272	1200	150
ks4284 – 85	14.08.2011	5788.274	900	140
ks4320 – 03	15.08.2011	5789.312	1200	200
ks4343 – 44	03.09.2011	5808.198	1200	200
ks4359 – 60	04.09.2011	5809.201	1200	180
ks4379 – 78	06.10.2011	5841.263	1200	150
ks4524 – 25	22.07.2013	6496.281	900	200
ks4554 – 55	25.08.2013	6530.448	900	220
ks4560 – 61	28.08.2013	6533.313	720	180
ks4577 – 78	29.08.2013	6534.34	720	180
ks4598 – 99	01.09.2013	6537.274	900	160
ks4662 – 63	20.09.2013	6556.363	900	180
ks4678 – 79	24.09.2013	6560.385	900	200
ks4740 – 41	03.10.2013	6569.243	900	200
ks4761 – 62	17.10.2013	6583.351	900	220
ks4776 – 77	18.10.2013	6584.382	900	200
ks4786 – 87	29.10.2013	6595.222	900	220
ks4795 – 96	04.11.2013	6601.24	900	180
ks4832 – 33	24.11.2013	6621.181	900	200
ks4861 – 62	25.11.2013	6622.194	1200	200
ks5243 – 44	19.06.2014	6828.177	900	160
ks5270 – 71	21.06.2014	6830.181	900	160
ks5309 – 10	26.06.2014	6835.194	900	180
ks5325 – 26	27.06.2014	6836.104	900	182
ks5338 – 39	03.07.2014	6842.104	900	160
ks5351 – 52	04.07.2014	6843.313	900	160
ks5367 – 68	11.07.2014	6850.354	900	170
ks5380 – 81	12.07.2014	6851.358	720	200

Continuation of the table 1

Spectrum	**Data**	**JD2455000+**	**Exposition time (sec)**	**S/N (at Hα)**
ks5391 – 92	16.07.2014	6855.368	720	200
ks5404 – 05	17.07.2014	6856.378	720	200
ks5461 – 62	23.07.2014	6862.382	720	220
ks5473 – 74	24.07.2014	6863.274	900	180
ks5490 – 91	25.07.2014	6864.309	900	180
ks5515 – 16	30.07.2014	6869.285	900	180
ks5540 – 41	05.08.2014	6875.271	900	200
ks5548 – 49	06.08.2014	6876.260	900	200
ks5569 – 70	07.08.2014	6877.306	900	180
ks5591 – 92	09.08.2014	6879.316	900	180
ks5604 – 05	10.08.2014	6880.299	900	180
ks5622 – 23	12.08.2014	6882.122	900	200
ks5737 – 38	18.08.2014	6888.326	900	220
ks59439 – 40	07.09.2014	6908.188	1200	240
ks6047 – 48	15.09.2014	6916.181	1200	240
ks6075 – 76	27.05.2015	7170.174	900	200
ks6088 – 89	30.05.2015	7173.163	900	220
ks6170 – 71	09.06.2015	7183.118	900	220
ks6192 – 93	11.06.2015	7185.129	900	240
ks6260 – 61	19.06.2015	7193.215	900	240
ks6298 – 99	21.06.2015	7195.222	900	200
ks6360 – 61	28.06.2015	7202.215	900	200
ks6399 – 6401	07.07.2015	7211.222	900	220
ks6412 – 13	08.07.2015	7212.264	900	220
ks6413 – 32	09.07.2015	7213.271	900	240

1. THE LINE Hα

1.1. Data for 2011

In the Fig. 1 (left panel) is demonstrated all profiles of the line Hα obtained in the time interval 02.07.2011 - 06.10.2011. Besides the strong photospheric lines C II λ6578 and 6583 Å, the remaining weak and narrow absorption components in this area are terrestrial atmosphericlines. These lines are helping to control the displacement in different spectra, and allow us to determine the wavelengths of the given echelle spectrum with an accuracy of $\pm$0.04 Å. As can be seen, there is a significant variations in the line profile for different dates. It is necessary to distinguish the following features of the Hα line profile in 2011: a) a variable central emission component showing either a single or a double peak, b) a broad emission above the continuum level, both in the red and blue wings of the line, c) a very wide absorption on the blue wing.

As can be seen from Fig. 1 (left panel), the central emission component of the line Hα in 2011 shows the profile variations for different dates. For example, from July 2, we have a single peak, which is observed until June 13 in such structure. Starting from July 13, there is a double peak with a stronger blue component. During the period from 21.07 to 15.08, that is, approximately 24 days there is a single peak. In the dates 03.09-06.10 a double peak with an intensive red component is observed. These results shows that the structure of the line profile can to be remain unchangeable for 25-30 days.

Fig. 1 (left panel) shows that in addition to the central part of the emission, in the red wing of the line Hα, a wide emission is observed. This emission is insignificantly higher than the continuum level, but extends quite widely, down to the telluric line H_2O of λ 6572.0704 Å. The value of the displacement of this emission at the red wing in different dates reaches up to 500-580 km s^{-1}. As a measure of this emission on the red wing, the equivalent width of the contour, bounded between telluric lines of H_2O λ 6563.5096 and 6572.0704 Å, was calculated. The value of the equivalent width of the wide part of the emission varies on different dates.

Only for three nights – in 02.07, 04.07 and 06.07, in the blue wing too there is a wide emission in the line Hα with an unusual displacement of up to -400 km s^{-1} (Fig. 1, left panel). In the time interval from 21.07 to 02.08, a very wide absorption is observed on the blue wing of the line. Here the maximum displacement of absorption component reaches -510 km s^{-1}. At 21.07 we immediately see a large value of the equivalent width of this absorption, which decreases for 17 days before complete disappearance. Unfortunately, we did not get to the initial phase of appearance of this absorption. Before to this event, the spectrum was obtained in 19.07, that is, two days before the appearance of the broad absorp-

tion. On this day there is no observed wide absorption on the blue wing. Hence it can be assumed that the wide absorption perhaps could beoccurred after the date of 19.07, and the maximum time between its appearance and disappearance is taking about 20 days.

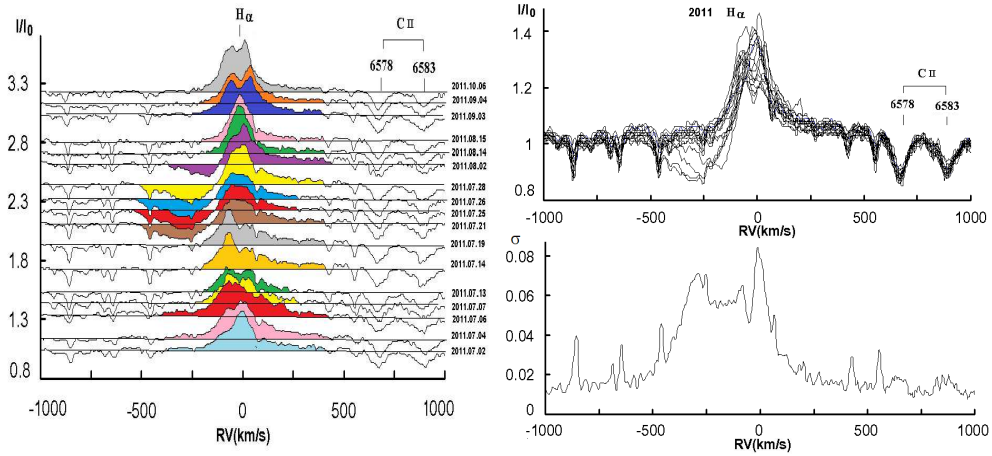

Fig. 1. The profile variability of the line Hα for different dates (left panel). The right panel shows the dynamic spectrum of the line profile Hα from observations of 2011, as well as the root-mean-square variation in intensity along the wavelength.

The right panel of Fig. 1 shows all the contours of the line Hα superimposed on each to other, and also in the lower panel the root-mean-square deviation versus the mean intensity along the wavelength. This figure shows that almost all parts of the profile shows variationfor different dates, and most often in the emission peak on the blue wingof the line.

In diagram is presented in the Fig. 2 it is showing the time variation of equivalent width of the broad absorption component Wab(b) and the wide emission component on the red wing Wem(r)in the line Hα. The black circles are representedemission data Wem (r) on the red wing, and the open circles – wide absorption Wab (b) data on the blue wing. The dotted line is the third-degree polynomial curve for the given emission component. As can be seen from Fig. 1, in 2011 a wide emission on the red wing is observed almost in all dates. In Fig. 2, the black circles show a smooth change in the parameter Wem (r) with time, which in the time interval from 07.07 to 02.08 shows an overestimated value of the equivalent width of this emission relative to other dates.

We note that the appearance and disappearance of the wide absorption on the blue wing is also observed in this time interval. As can be seen from Fig. 2, the wide absorption has the largest value of the equivalent width, when the equivalent width ofemission component is also reached a maximum. Then, both of these pa-

rameters are synchronous decreasing, and the blue absorption equivalent widths aredecreasing quickly thanin EW of the emission component (Fig. 2).

In Fig. 3 is shown the time variability of radial velocities (on the left panel) and equivalent widths (right panel) of the central emission component of the line Hα. As you can see, the equivalent widths are changing smoothly, which are passing through a minimum at 02.08.2011 (JD 2455776). The comparison of Fig. 2 and Fig. 3 shows that there is no definite relationship in the appearance of broad absorption and emission with variations in the radial velocities and equivalent widths of the central emission component of the line Hα.

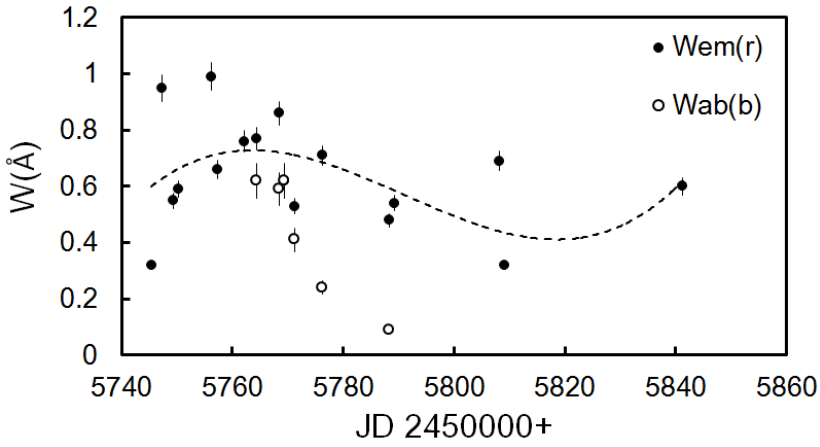

Fig. 2. Time variabilityof equivalent widths in 2011 of wide emission on the red wing (black circles) and wide absorption on the blue wing (open circles) for the line Hα. A dotted line is passed through black dots by the third degree of the polynomial.

As can be seen from Fig. 3, a smooth decrease in the equivalent width occurs in approximately 31 days, while its increase is over 65 days, i.e. twice as longer. The radial velocities show a variation within 20 km s^{-1}, and equivalent widths of 1.3 Å.

1.2. Results for 2013

In the Fig. 4 is shownthe same as in the Fig. 1, obtained from the data 2013 for the line Hα. As can be seen from Fig. 4, in 2013, the profiles of the line Hα have two central emission peaks with a stronger blue component. The red emission component sometimes is very weak and is hardly detected from the noise. For example, at 29.10.2013 and 04.11.2013 only a single emission component is observed. In addition, in the 10.10.2013 to 18.10.2015 the appearance of the wide emission on the red and blue wings is revealed, and it has a maximum value of

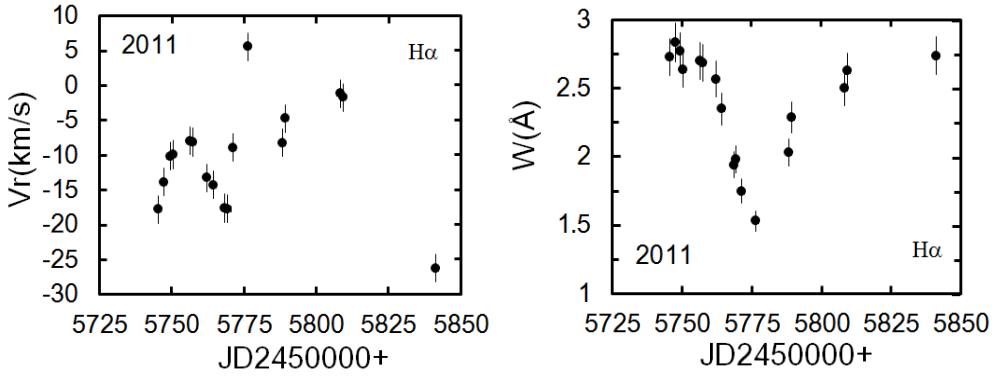

Fig. 3. Time variabilityof equivalent widths in 2011of wide emission on the red wing (black circles) and wide absorption on the blue wing (open circles) for the line Hα. A dotted line is passed through black dots by the third degree of the polynomial.

the equivalent width at 17.10.2013 of about 0.33 ± 0.04 Å. Also on this date, the edge of emission line wings has a maximum displacement of - 480 to +470 km s^{-1}. We can note that the time interval for the appearance of a wide emission and its disappearance is taking at least 15 days.

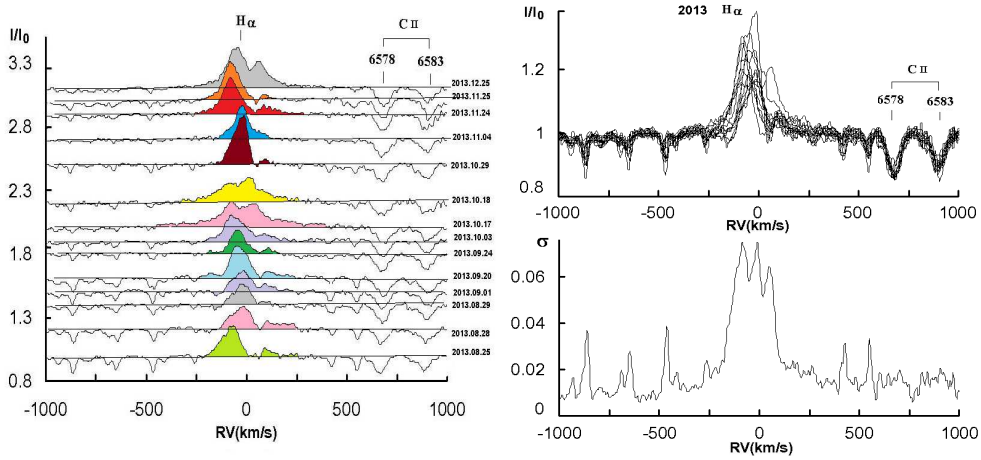

Fig. 4. The same as in Fig. 1, according to data for 2013 for the line Hα.

As can be seen from the right panel of Fig. 4, the line profile is variable, with variability being observed both in the central sections and in the line wings. It is interesting that in 2013 there is practically no absorption component in the line Hα.

In the Fig. 5 is presented the time variation of radial velocities and equivalent widths of the central emission component of the line Hα. As can be seen from

Fig.5, an increase of equivalent widths to a maximum is occurred in 88 days, while a decrease is occurred in about 35 days. Radial velocities are varied within range 80 km s^{-1}, and equivalent widths, at 0.5 Å.

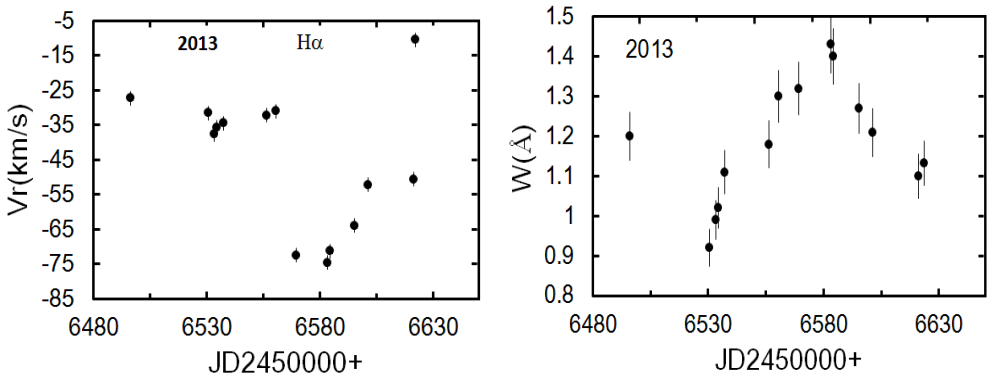

Fig. 5. The same as on the Fig.3 for the data of 2013.

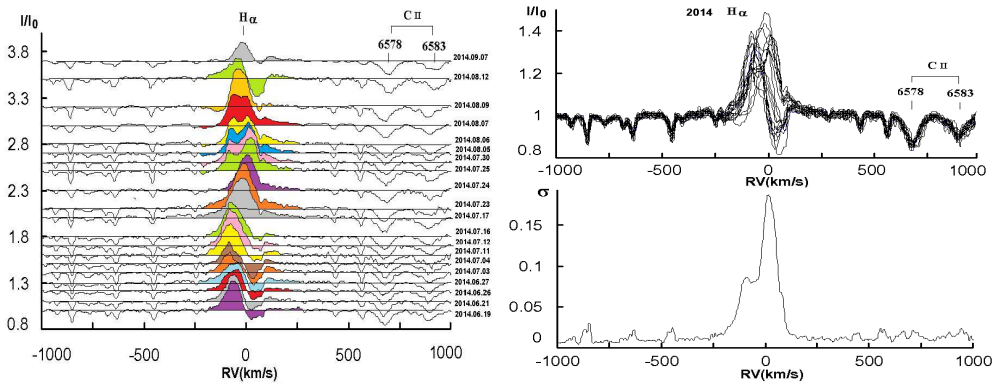

Fig. 6. The same as on the Fig.1 for the data of 2014.

1.3. Results for 2014

In the Fig. 6 is shown the profiles of the line Hα obtained in 2014. As can be see, this year is observed the invers-P Cygtype profilespredomination, that is, strong emission on the blue wing and the absorption component on the red wing of the line. The equivalent width of the central absorption and emission varies from night to night. From 19.06.2014 to 16.07.2014 for about 27 days, absorption on the red wing is stable observed. For 7 nights from July 17, 2014 to July 24, 2014 there is a single wide emission peak with wide emission wings. From 25.07.2014 to 07.08.2014, i.e. within 12 days a double emission peak with

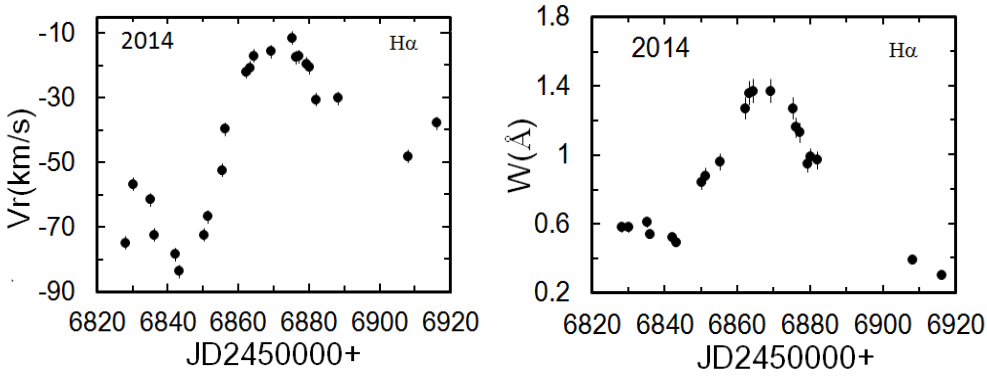

Fig. 7. The same as in Fig. 3 on the data of 2014.

a stronger red component is observed. The last three dates of the season from 09.08.2014 to 07.09.2014 are again observed profiles with absorption on the red wing. The displacement of the wide emission reaches in the blue and red wings -375 km s^{-1} and +400 km s^{-1}, respectively.

The right panel of Fig. 6 is shown that the strongest variations are observed on the red wing of the absorption component of Hα. On the diagrams presented in the Fig. 7 the time variability of radial velocities and equivalent widths of the central emission component of the line Hα. As can be seen, there is a smooth change in the radial velocities and equivalent widths. This is the unique case of the four observation seasons that we have, whenvariability of radial velocities and equivalent widths of emission in the line Hα are synchronized. As can be seen from Fig. 7, both radial velocities and equivalent widths have their minima at 04.07.2014, and both parameters are reaches a maximum at 30.07.2014, i.e. for about 26 days. Equivalent widths further decrease and in about 47 days are reaches a minimum. The total amplitude of the radial velocity variation from peak to peak is about 80 km s^{-1}, and the equivalent widths are about 1.2 Å.

1.4. Results for 2015

In the Fig. 8 the Hα line profiles obtained in 2015have been demonstrated. In these spectrums intensivewide emission components along the line wings is more characteristic. Starting from June 28, 2015 to July 09, 2015, i.e. in about 11 days, a wide emission was significantly strengthened. Unfortunately, after 09.07.2014, the observations were not continued and we do not know the further nature of variability in thewide emission. The maximal displacementof the wide emission on the wings at the continuumlevel reaches -600 km s^{-1} in blue and 540 km s^{-1}

in red wings. At maximum, the total equivalent width of emission component reachesto 2.25 Å.

In the Fig. 8 is seen that the central emission component in the line have demonstrated a significant variability from night to night. For example, in the night from 27.05.2015 to 11.06.2015, the line profile exhibits a multicomponent structure and very weak emission and absorption, hardly distinguished from the noise. After June 19, 2015 there is a gradual increase in the intensity of the emission component, which reaches a maximum on July 9, 2015. Simultaneously, a considerable expansion of the wings of this emission is observed.

On the left panel of the Fig. 9 is shown the time variationsof borders of this emission, where the black circles is indicating of red, and open circles of blue borders of the wide emission. The second panel in Fig. 9 shows the change in the total value of the equivalent width of wide emission including all emission components. As can be seen, when is increasing the equivalent width of emission, is also observed synchronal increasing in the displacement of border velocities of the line wings. As can be seen from Fig. 9, the variability of the line wings and the intensity of the emission peak is carried a symmetric and synchronous behavior.

2. THE LINE Hβ

The profile of the line Hβ is a broad absorption with a half-width that reaches an average of 2-3.5 Å. Figure 10 shows the dynamic of profiles of the line Hβ obtained in different years, as well as the standard deviation of the intensity versus from the line displacement. The displacement of the absorption peak is often close to zero, but according to observations in 2015, a shift to the red part was obtained about +100 km s^{-1}.

In different years there is anemission component, often superimposed on the blue wing and on the peak of the line. Rather, the apparent peak shift arises from distortion of the profile by additional emission component, which is superimposed on the blue wing extending up to the center of the line. This is especially noticeable in the dynamic profiles of Hβ given for 2014 and 2015 in the Fig 10. The maximum shift of the emission component sometimes reaches -300 km s^{-1}, but often corresponds to -100 km s^{-1}.

As can be seen from Fig.110, only in one night, namely on 29.10.2013, a narrow emission peak with practically without displacement is observed in the center of the absorption line Hβ. On the same night, the Hα line also shows a strong and narrow emission structure, without any absorption components. This observational fact will be reported in more detail in another paper.

As seen in Fig.10, where is presented the structure of the standard deviation σ from the average intensity, practically all years are identical with the structure

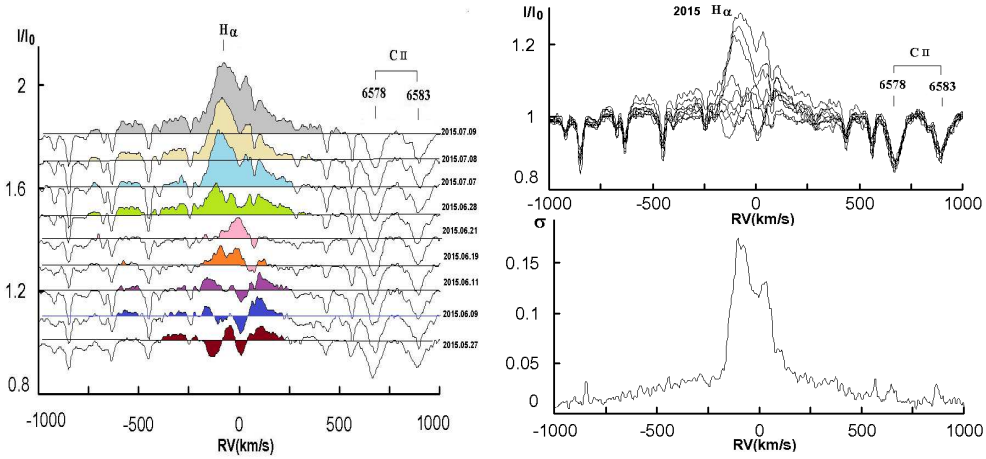

Fig. 8. The same as on the Fig.1 for the data of 2015.

of σ obtained for the line Hα. As can be seen from thediagram of structure α, unlike the line Hα in the line Hβ on the red wing, traces of the emission component are practically never observed. This indicates that in the deeper layers of the atmosphere, where the Hβ line is formed, only the outflow of matter from the star is observed. On the upper layers where more probably is arousing the line Hα, both the outflow and the accretion of the matter are observed.

The HVA event which was observed on the blue wing near the line Hα alsoin 2011 the same time wasobserved on the blue wing of the line Hβ (Fig. 10). The maximum displacement of absorption at the continuum level on individual days reaches -500 km s^{-1}. This indicates that the acceleration of the stellar wind also is occurred in the deeper layers of the atmosphere, where the Hβ line is formed.

In the Fig. 11 is shown the graphs of the variations in radial velocities and the equivalent widths of absorption in the line Hβ. As can be seen from Fig. 11, according to 2011, the maximums of W_λ are accompanied with a minimum of Vr. However, unlike the Hα line in 2013 and in 2014, there is clearly no coincidence of the extrema of these parameters. According to the results of observations in 2015, we obtained a smooth decrease in the equivalent widths, as well as a smooth shift of the emitting layer of matter to the observer.

As can be seen from Fig. 11, the general character of the parameters variability of the absorption line Hβ (smooth variation and the appearance of extremes with a characteristic time of 20-25 days) is generally similar in the parameters variation of the emission component of the line Hα. This indicates that the atmospheric layers, where absorption Hβ is formed, has a close influence to the variability in the upper layers, where the emission in the line Hα is formed. Our observations showed that the parameters of the Hα and Hβ lines show smooth increasing and

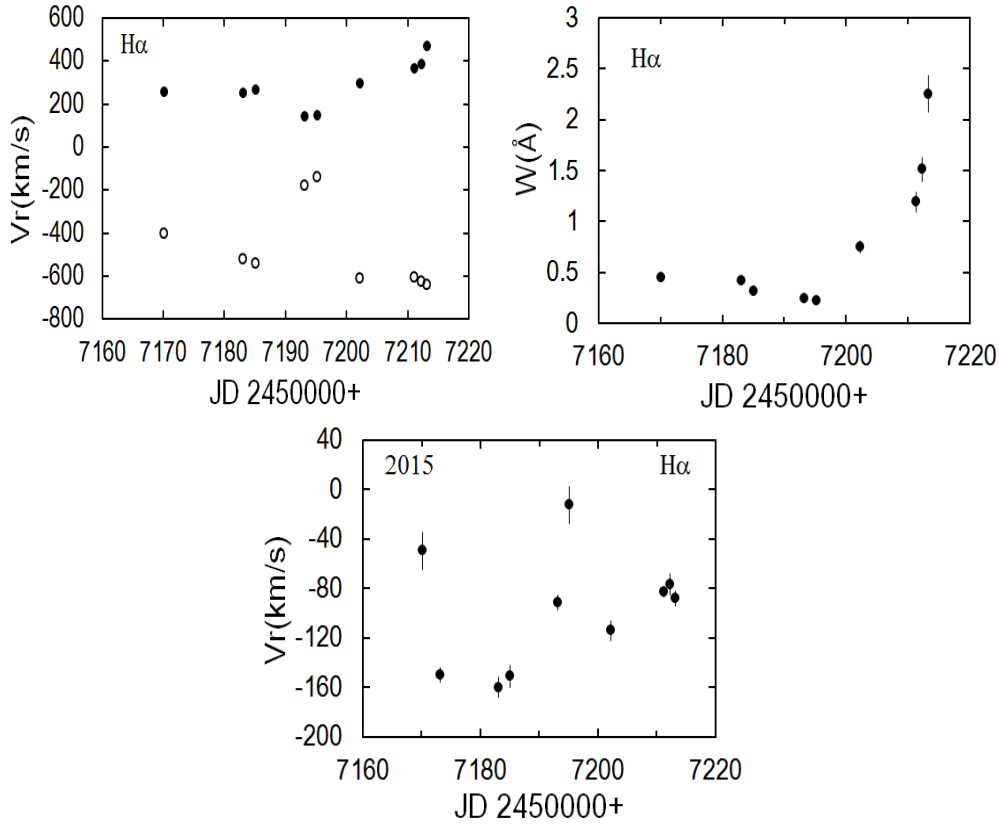

Fig. 9. On the left panel – time variations of border velocities of red (black circles) and blue (light circles) components of wide emission for the line Hα. In the right panel– variations of equivalent widthsof the wide emissionfor the same dates. The displacement in time of the strongest central emission peak is shown below.

decreasing cycles with a well-marked maximum or minimum of these parameters. This is especially noticeable for the values of the equivalent widths.

In the Table 2 have presented the intervals of wave-like increasing or decreasing of the equivalent widths of hydrogen lines Hα and Hβ. The Table 2 contains the following parameters: t1- the beginning of the cycle (in JD 2450000+), t2 is the date of the maximum or minimum points, t3 is the cycle end date, Δt1 is the number of days from the beginning of the cycle to the extremum point, Δt2 is the number of days from the extremum point up to the end of the cycle, Δt is the total cycle time. We have chosen the data in which the cycles of variation W_λ are surely was discovered. In the Table 3 is presented the amplitudes of the variations from peak to peak radial velocities and equivalent widths of the line Hα for both emission and absorption components and for Hβ absorption. The

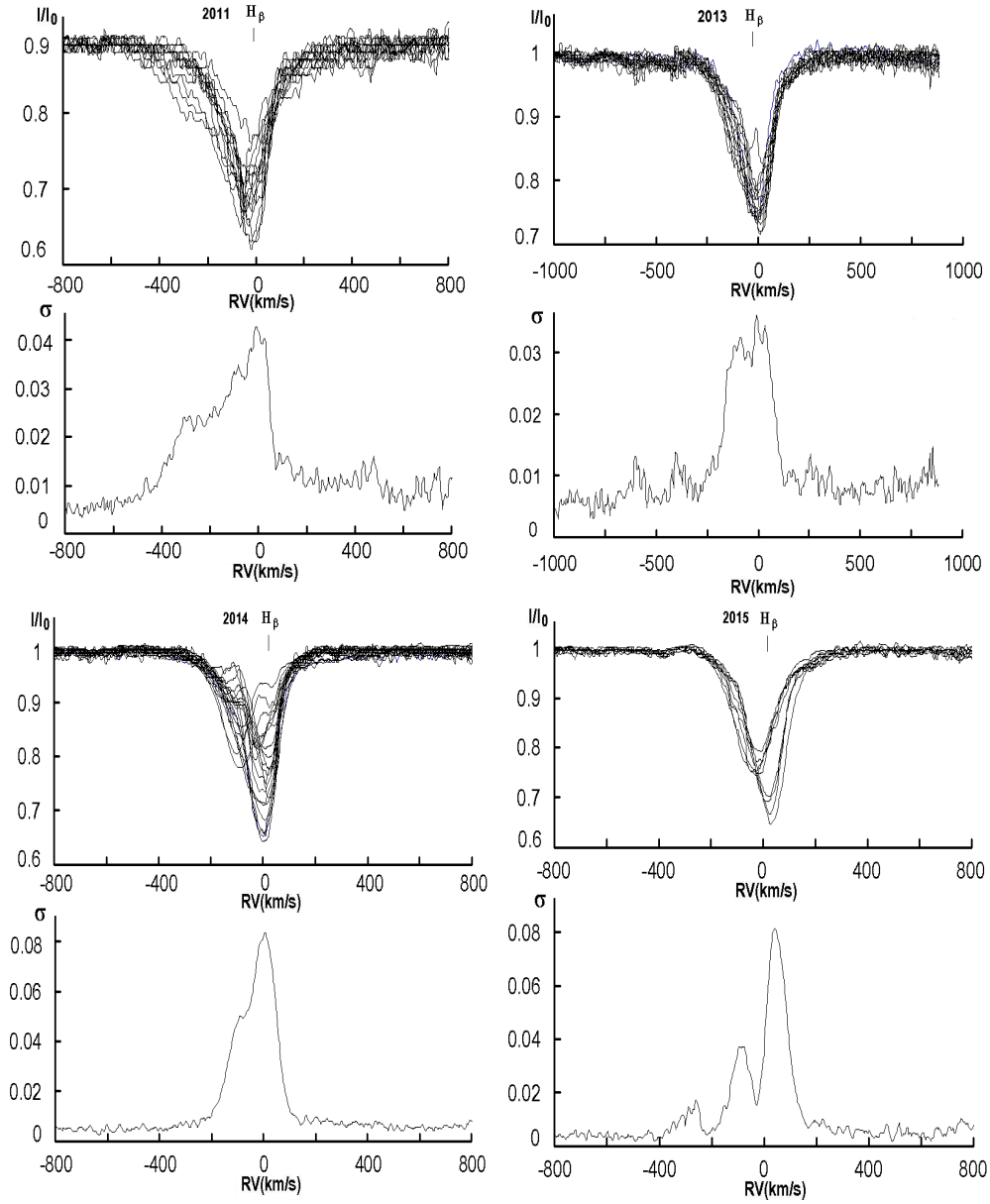

Fig. 10. Profiles of the line Hβ in 2011 and 2013-2015. In the second part of each figure, the standard deviation σ from the average of the relative intensity at the given displacement is presented.

time interval Δt is also given there, during which the corresponding parameters decreases or increases from peak to peak. As can be seen from Table 3, in average, the amplitudes of variability in the emission component of Hα are greater than

for the absorption in the line Hβ. Moreover, the maximum value of the amplitude of variations in Vr of hydrogen lines is within the range of 30-60 km s^{-1}, and the characteristic time of variability of Vr and W_λ is approximately close and are in the range from 11 to 53 days. Data for the parameter Δt from Table 3 showed that for the total 14 events with the appearance of an extremum in the parameterchange, the average characteristic time in the interval 20-25 days is observed in the 6 (about 43%) case, which on the mean is 22 days. This is in good agreement with the characteristic time of 20 days given in the work [12]. All other values of the parameter Δt are not repeated for different events. The results of this analysis is demonstrated on the diagram of the distribution of the parameter Δ t, obtained from different variability events of the parameters (Fig. 12). The abscissa shows the intervals in days, with a step of 5 days. The ordinate shows the relative number of events N with an extremum to the total number of events No = 14 in a given interval. As can be seen from Table 3 and from the diagram in Fig. 12, the most probable number of events with an average characteristic time of 22 days is observed in the interval of 20-25 days.

Table 2. Time intervals of variability of the parameters W_λ of lines Hα and Hβ for diffeent years.

Hα	**2450000+**			**days**		
years	t1	t2	t3	Δt1	Δt2	Δt
2011	5747	5776	5841	29	65	94
2013	6530	6583	6621	53	38	91
2014	6842	6869	6916	27	47	74
2015	7202	7213		11		
Hβ	**2450000+**			**days**		
years	t1	t2	t3	Δt1	Δt2	Δt
2011	5747	5768	5841	21	73	94
2013	6496	6537	6601	41	64	105
2014	6835	6864	6882	29	18	47
2015	7170	7193	7212	23	19	42

Note: Table 2 contains the following parameters: t1 is the cycle start date (in JD 2450000+), t2 is the date of the maximum or minimum point, t3 is the cycle end date, Δt1 is the number of days from the beginning of the cycle to the extremum point, Δt2 is the number of days from the extremum point to the end of the cycle, Δt is the total cycle time.

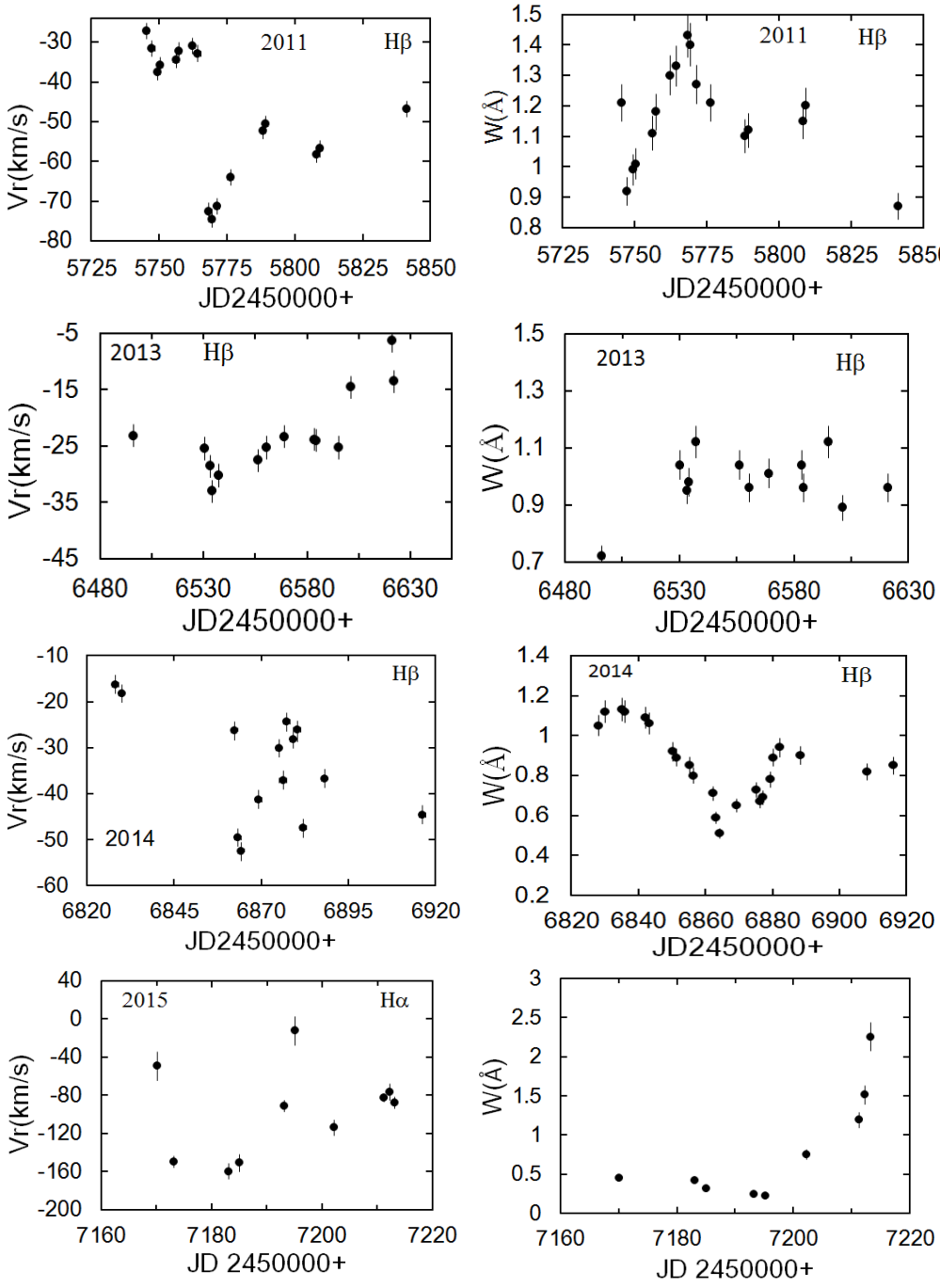

Fig. 11. Time variability in the radial velocities Vr and the equivalent widths W_λ of the absorption line Hβ for different years.

Table 3. Amplitudes of changes from peak to peak of equivalent widths and radial velocities of Hα and Hβ lines for different seasons.

Years	ΔVre(Hα) km s^{-1}	Δt, days	ΔWe (Hα), Å	Δt, days	ΔVr(Hβ), km s^{-1}	Δt, days	ΔW (Hβ), Å	Δt, days
2011	31	24	1.5	31	40	20	0.5	21
2013	65	23	0.5	53	30	35, 87	0.35	5, 11
2014	72	32	0.9	21	28	13	0.75	29
2015					54	23	0.6	43

Note to Table 3. ΔVre(Hα) -radial velocity of central emission component of Hα, ΔWe(Hα) -equivalent widths of central emission of Hα, ΔVr(Hβ) -radial velocity of Hβ absorption component, ΔW(Hβ) -equivalent widths of the line Hβ. Δt is the total characteristic time of changes in the corresponding parameter.

As can be seen from Table 2, most probable cycles are completed in about 94 days or less, and it is impossible to determine which part of the curve occurs longer - to the extremum point or after it.

3. CONCLUSIONS

Our observations showed that the hydrogen lines Hα and Hβ most often are changing with a characteristic time of about 20-25 days. By using Fourier analysis for the variability of the line parameters of Hα was detectedperiods of 27.7 and 55.5 days [12]. Our observations showed that 20-29 days is observed as a characteristic time of variability (Table 3). Since the obtained time is not stable in different years, it is not irrelevant to assume about the existence of a stable periodic processes. Rather, we can talk a quasi-cyclic variability.

Can such a quasi-cyclic variability be due to the result of the axial rotation of the star? If we use the radius of the star 68 $R_{\odot}$, aspresents in [12], and in assuming that the period of axial rotation of the star is equal to the average characteristic time of 22 days obtained in this work, then for the absolute value of the rotation velocity of the star we can get 157 km s^{-1}. According to our calculations, the escape velocity V_{esc} for this star has a value of 224 km s^{-1}. This means that even if the star does rotate so fast, the stellar matter could not leave the system.

According also to the data [13], the projection of the rotation velocity to the line of sight is vsini = 41 km s^{-1}. The half-widths of the photospheric lines CII $\lambda\lambda$ 6347 and 6371 ÅÅ measured by us give a value of 0.8 $\pm$ 0.1 Å, which also gives about 40 km s^{-1}. Then for the angle i we would get the value 15°; in fact, we would have seen a star from the pole.

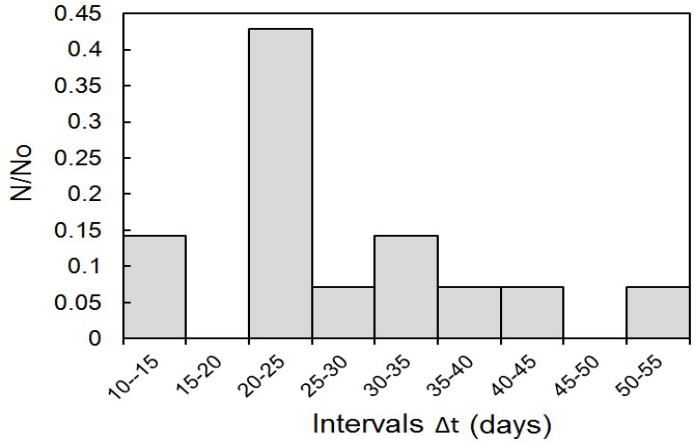

Fig. 12. The diagram of the Δt parameter distribution for different quasi cyclic events. The abscissa have presented intervals in days, the ordinate has a relative number to the total number of events in a given interval.

Our estimates show that the characteristic time of 22 days, rather, is not a period of rotation. On the one hand, in fact, activity in the star's atmosphere should be occurring most often, in the equatorial part. On the other hand, despite the fact that the characteristic time of 22 days is revealed from the data of observations of different authors, it is not observed as strictly stable. It is not excluded that the observed undulating variation of the radial velocities and equivalent widths of the components of the line Hα might be a consequence of radial pulsation.

As can be seen from the structure of the profiles of the Hα and Hβ lines, the motion of matter in the star's atmosphere can acceleratefrom 100 to 500 km s^{-1} relative to the surface of the star. The displacement of the individual emission components in the Hα line is symmetric with respect to the center of mass of the system and is about $\pm$30 km s^{-1}. The central absorption in the line Hα sometimes shows a blue shift up to -250 km s^{-1}, and a red shift up to +40 km s^{-1}. This may be due to the motion of matter in the circumstellar shell of the star.

So, based on the results of this work, we can make the following conclusions:

1. In the spectral line Hα ofthe supergiant HD199478 for 2011 was revealed weak wide emission components on the red and blue wings, as well as high velocity absorption (HVA) on the blue wing with the displacement of more than 500 km s^{-1}.

2. The characteristic time of variation was observedapproximately 20 days forthe wide emission and absorption components. In 2011, a wide emission and absorption events practically appear and disappear synchronously. In 2015 wide

emission component is enhanced, but HVA is not observed. In 2013 and 2014 both of these phenomena was not observed.

3. The most probable characteristic time of variability in the parameters of the spectral lines Hα and Hβ is 22 $\pm$ 2 days.

4. The observed variability in the atmosphere of the starprobably is not related to the axial rotation and the structure of the atmosphere, but may be the result of pulsation is occurred in the upper layers of the stellar atmosphere.

REFERENCES

1. Kaufer, A., Stahl, O., Wolf, B., etal. Long-term spectroscopic monitoring of BA-type supergiants. II. High-velocity absorptions in β Ori and HD96919.1996a, A&A, 314, 599

2. Kaufer, A., Stahl, O., Wolf, B., etal.Long-term spectroscopic monitoring of BA-type supergiants. I. Hα line-profile variability. 1996b, A&A, 305, 887

3. Kaufer, A., Stahl, O., Wolf, B., et al. Long-term spectroscopic monitoring of BA-type supergiants. III. Variability of photospheric lines. 1997, A&A, 320, 273

4. Denizman, L., Hack, M., Spectra and radial velocities of white supergiants. 1988, A&AS 75, 79

5. Rosendhal, J.D. A survey of H-alpha emission in early-type high-luminosity stars.1973, ApJ, 186, 909

6. Bates, B., Halliwell, D. R., Brown-Kerr, W.Ultraviolet spectroscopy of mass loss from late B-type supergiants. 1986, Irish Astron. Journal, 17, 256

7. Markova, N., Prinja, R. K., Markov,H. et al. Wind structure of late B supergiants. I. Multi-line analyses of near-surface and wind structure in HD 199 478 (B8 Iae)2008, A&A, 487, 211

8. Percy, J.R., Harlow, J., Haynoe, K.A.W.Photometric Monitoring of Bright Be Stars. III. 1988-89 and 1992-95. 1997, PASP,109, 1215

9. Mikailov, Kh. M., Khalilov, V. M., Alekberov, I.A.2005,Tsirk. ShAO, 109, 21

10. Ismailov, N. Z., Bahaddinova, G. R., Kalilov, O. V., Mikailov, Kh. M. Spectral Variability of IL Cephei. 2013, Astrophysical Bulletin, 68, 2, 196

11. Галазутдинов 1992. Г.А. Препринт САО РАН, 92,

12. Markova, N., Valchev, T. Spectral variability of luminous early type stars. I. Peculiar supergiant HD199478. 2000, A&A, 363, 995

13. Markova, N., Puls, J. Bright OB stars in the Galaxy. IV. Stellar and wind parameters of early to late B supergiants.2008, A&A, 478, 823

HD199278 İFRATNƏHƏNGİN SPEKTRİNDƏ YÜKSƏKSÜRƏTLİ UDULMA VƏ ŞÜALANMA

Ş. K. İsmayılova, N. Z. İsmayılov, X. M. Mikayılov

N.Tusi adına Şamaxı Astrofizika Rəsədxanası,
Azərbaycan Milli Elmlər Akademiyası, Şamaxı rayonu, Azərbaycan

HD199478 (B8Iae) ifratnəhəng ulduzunun spektrində Hα və Hβ xətlərinin monitorinqinin nəticələri verilmişdir. Spektral müşahidələr əsasında bu ulduzda müşahidə olunan və fiziki təbiəti hələ məlum olmayan qeyri-adi geniş şüalanma və yüksəksürətli absorbsiya fenomeninin tədqiqi yerinə yetirilmişdir. Bizim müşahidələr göstərdi ki, baxilan xətlərin profillərinin ümumi strukturutəqribən 18-24 gün ərzində dəyişməz qalır. Müxtəlif 4 ilin müşahidələri göstərdi ki, baxılan xətlərin parametrləri ciddi periodik dəyişmə göstərmir. Hidrogen xətlərinin parametrlərinin ən ehtimallı xarakterik dəyişmə vaxtı 22$\pm$2 gün təşkil etmişdir. Yalnız 2011-ci ildə bir sezonda -510 km s^{-1} sürüşməyə malik olan geniş absorbsiya aşkar edilmişdir. Hα xəttində göy qanadda müşahidə olunan geniş absorbsiyadan fərqli olaraq daha çox müşahidə olunan geniş şüalanma strukturunun sürəti $\pm$ 500 km s^{-1} çatır.

Açar sözlər: Baş ardıcıllıq ulduzları – Spektral və fotometrik aktivlik – maqnit sahələri

SPECTROSCOPIC VARIABILITY OF THE SUPERGIANT STARS HD 21389 AND HD 187982

***Ya. M. Magerramov*[*], *A. R. Hasanova*, *A. M. Khalilov*,**

A. Sh. Baloglanov*, *G. M. Hajiyeva

Shamakhy Astrophysical Observatory named after N.Tusi,
Azerbaijan National Academy of Sciences, Shamakhy region, Azerbaijan

In this paper, we study the structure and spectral parameters of the profiles Hα, Hβ, HeI (5876 Å) and NaID lines in the spectra of the supergiant stars HD21389 and HD187982 obtained in 2005-2006 and 2013-2015 in the Shamakhy Astrophysical Observatory (ShAO). It was found out that in the spectrum of HD21389, the Hα absorption has a complex structure depending on the phase of instability of the star atmosphere. In the active phase, this line shows an inverse PCyg profile. The emission components appear and disappear on the red and violet wings of the profile. All the measured parameters of the lines Hα and Hβ, demonstrate variability.

It is assumed that these changes occur due to the non-stationarity and outflow of matter from the atmosphere of these stars. The appearance and disappearance of the asymmetry in the profile of the NaD doublet line and the formation of the inverse PCyg profile of Hα line in the atmosphere of the supergiant HD21389 occur synchronously. In the spectrum of the supergiant HD187982, the emission components appear and disappear in red wing ofthe profile Hα.This line has a normal PCyg profile in the active phase of the star atmosphere. All the measured parameters (V_r, W, R) of the lines Hα, Hβ and the FeII line in 2013-2015 show variability for a month or less. The parameters changing occur sometimes synchronously, and sometimes occur in anti-phase. All these facts indicate that there is a matter flow in certain layers of the atmosphere of HD187982 where these lines are formed, the direction and velocity of the matter flow change and pulsation type movements are observed.

Keywords: Supergiants-stars – Pulsation

[*] E-mail: y_meherremov@rambler.ru

ation Cam OB1. The authors of [1, 3–5]calculated some parameters of the star: $\log g$=1.70, $M_*/M_\odot = 19.3$, $R_*/R_\odot = 97$, $\log(L_*/L_\odot) = 4.87$. For the fundamental parameters of the star as well as atmosphere, temperature, mass and radius, different authors obtained different from each other, but close values Teff=11000 K, 9730 K and 10100 K; $M_*/M_\odot = 14$, $M_*/M_\odot = 16$, $R_*/R_\odot = 104.2$, $R_*/R_\odot = 99$ [3, 4, 6, 7].

According to the spectra of the star HD21389, the lines Hα, Hβ, Hγ, Hδ, Hε, HeI (4471, 4921, 6678 Å), SiII (3853.6, 3856, 3862.5 Å), NaI (D1 and D2), MgII (4481 Å), DIB (5797, 5780, 5850, 6614 Å), OI (6156, 6157, 6158 Å), CII (4267 Å), FeII (4923.9, 6147.7, 6149.3 Å) have been studied [5,8–14]. It is revealed that for this star the profile of the line Hα has a complex structure and is observed in the following forms:

a) the normal P Cyg profile;

b) inverse P Cyg profile with a weak emission component in the violet wing;

c) pure absorption profile;

d) pure emission profile;

f) the weak emission components are observed on the red and violet wings of the absorption line Hα.

It was found out that in the spectrum of the supergiant HD21389 the form, equivalent width, line depth, radial velocity and other parameters of the line Hα show a strong change with time. The equivalent width varies from 0.09 Å to 0.45 Å, i.e. almost five times [7, 15].

It was noted in [8–11,13,14,16,17] that according to the spectrograms obtained on the same night, only in two cases the line Hα shows strong rapid changes (the radial velocity has changed from -54.8 km s^{-1} to -46 km s^{-1}). The same authors note that the shape and type of the profile of the line Hβ, as well as its other parameters, show strong changes. Sometimes a weak emission component can be traced in the profiles of the line Hβ. In [8], the time variation of the radial velocities and differential shifts of the lines of ions, hydrogen, and helium in star HD21389 were studied. The dependence of the radial velocities on the depth of the formation of lines is noted. That indicates the presence in the atmosphere of HD21389 motions such as radial pulsations. The maximum recorded line shifts corresponding to the compression and expansion are close to +10 and -20 km s^{-1}, respectively. The authors of [13, 18] carried out a study of the atmosphere of this star on the basis of measuring the radial velocities of the lines along the optical depth. It turned out that the radial velocity, determined from the lines Hα, Hβ,

HeI, SiII varies in the optical depth. These changes they explained by pulsations occurring in the atmosphere of this star.

Star HD187982. The star HD187982 (A2Ia; $m_v = 5^m.58$; $T_{eff} = (9300 \pm 250)$ K; $v \sin i = (15 \pm 6)$ km s^{-1}) is a supergiant of the type PCyg, and belongs to the associations Vul OB4 and $\log g$=1.60±0.15, $M_*/M_\odot = 15$, $R_*/R_\odot = 78$ [3, 19, 20]. The supergiant star HD187982 has been little studied spectrally. In the works of a number of authors, the profiles of the lines Hα, $H\gamma$, MgII(4481 Å), DIB(5780 Å) and FeII(4924, 5018, 5169 Å) in the spectra of this star have been studied [3,12,21,22]. It is noted that the profiles of the line Hα are observed mainly in a purely absorption. Sometimes a weak emission component is observed on the red wing of the profile. Hα. The appearance and disappearance of this component has not yet been fully explained.

Thus, the study of supergiant stars HD21389 and HD187982 is interesting and relevant from the point of view of studying the nature of the changes in the profile of the lines Hα, Hβ, $H\gamma$ etc. in the spectra of these stars.

In our work, the profiles of the lines Hα, Hβ, HeI (5876 Å), sodium doublet NaID, FeII, etc. are presented and discussed according to the spectrograms obtained at the 2-nd telescope of the ShAO.

2. OBSERVATION AND THEIR PROCESSING

The spectral observations of the stars HD21389 and HD187982 were performed in the periods 2005-2006 and 2013-2015, in the Cassegrain focus of the 2nd telescope of the ShAO of the Azerbaijan National Academy of Sciences using the echelle spectrometer collected on the basis of the UAGS spectrograph [23]. As a detector, a CCD with 530×580 elements was used. On each observational night, two spectra of the star were obtained. The average exposure is 600 seconds, depending on the image quality. Quick changes during the night were not detected. Therefore, the profiles obtained overnight were averaged.

In order to study the stability of the apparatus and the telescope-receiver complex, many spectra of standard stars were simultaneously obtained, as well as the level of the dark background, the flat field, and the comparison spectrum. For the construction of dispersion curves, the sky spectrum was used. In addition, for all spectrograms, heliocentric corrections are taken into account.

The profiles of Hα, Hβ, HeI and other lines in the spectrum of the supergiant stars HD213389 and HD187982 were investiaged.The obtained spectra were processed by the DECH20 and DECH20T software package [24]. The measurement errors for the radial velcities were ±2 km s^{-1}, and for the equivalent widths did not exceed 10%.The resolution was $R \sim 15000$, the spectral range $\lambda\lambda 4700 - 6700$ ÅÅ, $S/N \sim 150 - 200$.

HD21389. The spectra obtained in 2005, 2006 and 2014 were investigated. A change in the profile of the lines Hα and Hβ was observed.The stucture of the profiles and the values of the radial velocities and spectral parameters of the lines Hα,Hβ,HeI and the doublet of NaID ara presented (Fig. 1, 2, 3).

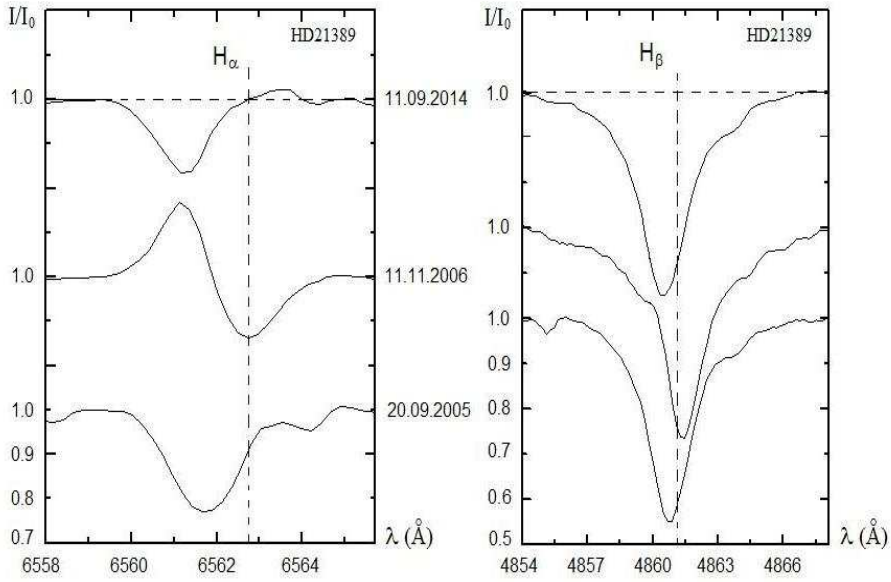

Fig. 1. The profiles of the Hα and Hβ lines in the spectrum of the supergiant HD21389, obtained at different times.

It can be seen from Fig. 1 that in the spectrum of the supergiant star HD21389 the profile of the line Hα is observed to be purely absorptive on September 20, 2005, and the line profile is observed in the shape of the inverse and normal PCyg profile in 11.11.2006 and 11.09.2014, respectively.

As can be seen from Table 1, on September 20, 2005 the radial velocities determined from the lines Hα and Hβ, are -29 km s^{-1} and -14 km s^{-1}, respectively. However, on 11.11.2006 the radial velocities strongly differ from the values obtained on September 20, 2005. The radial velocity of the Hα line in the absorption is +4 km s^{-1}, and in the emission -69 km s^{-1}. Changes in the Hα line in absorption are 7-12 times different with respect to 20.09.2005 and 11.09.2014, respectively.

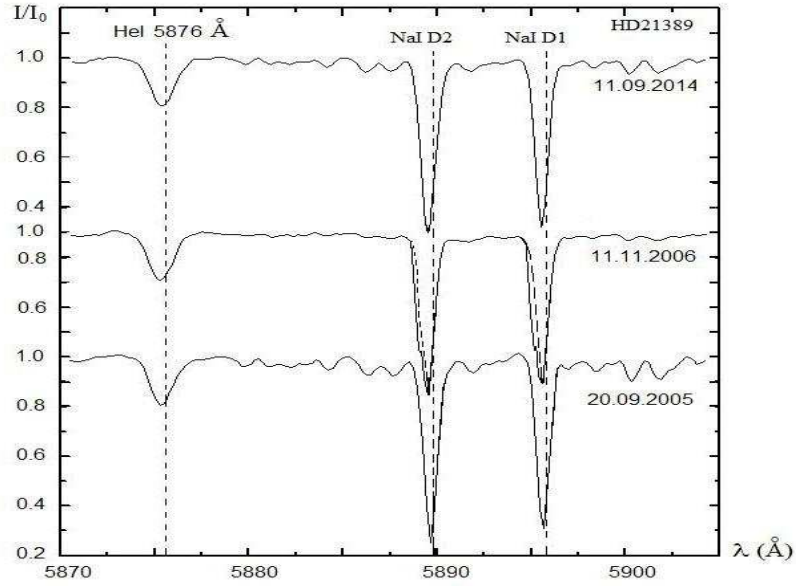

Fig. 2. The profiles of the HeI (5876 Å) and NaID doublet lines in the spectrum of the supergiant HD21389, obtained at different times.

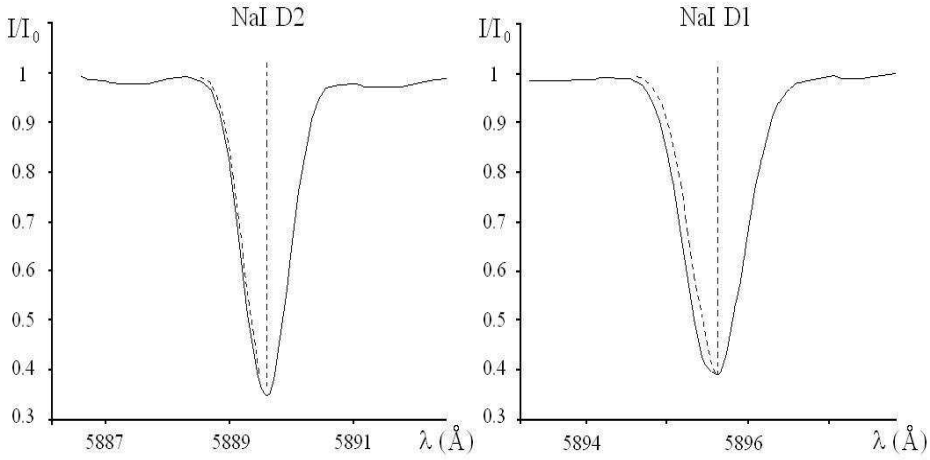

Fig. 3. The profiles of the NaID doublet line in the spectrum of the supergiant HD21389, obtained in 11.11.2006

Table 1. Results of the measurements of the radial velocity and spectral parameters of the lines Hα, Hβ, HeI and sodium doublet NaID in the supergiant star HD 21389

Date	HD21389											
	Hα (abs)				Hα (em)				Hβ			
	Vr kms^{-1}	WÅ	$\Delta\lambda_{1/2}$	R	Vr kms^{-1}	WÅ	$\Delta\lambda_{1/2}$	r_v	Vr kms^{-1}	WÅ	$\Delta\lambda_{1/2}$	R
20.09.2005	−29	0.48	1.7	0.23	–	–	–	–	−14	1.39	2.4	0.45
11.11.2006	4	0.19	1.3	0.14	−69	0.19	1.1	1.17	10	1.68	2.2	0.47
11.09.2014	−49	0.39	1.5	0.19	–	–	–	–	−30	1.55	2.7	0.45

Date	HD21389							
	HeI				NaI Da1		NaI Da2	
	Vr kms^{-1}	WÅ	$\Delta\lambda_{1/2}$	R	Vr kms^{-1}	WÅ	Vr kms^{-1}	WÅ
20.09.2005	−8.2	0.32	1.4	0.20	−8.3	0.58	−8.4	0.70
11.11.2006	−8.3	0.31	1.5	0.19	−10.8	0.58	−11.3	0.62
11.09.2014	−8.0	0.33	1.6	0.19	−10.6	0.61	−11.4	0.70

Such a strong change in the value of the radial velocity indicates a powerful physical process taking place in the atmosphere of this star. It is assumed that due to stellar wind and pulsations, mass is outflowed from the star's atmosphere. Part of this mass goes into the interstellar medium, and some of this mass forms an envelope around this star. However, when a substance is released from the star, not all of the mass outflows the star, some of the ejected gas cools and falls back to the surface of the star. Depending on the velocity and mass of the incident substance, this can affect the absorption component of the line Hα which appears in the atmosphere of the star. The presence of emission details in the violet part of the profile may indicate the presence of movement of the substance in the direction from the observer, and the presence of absorption details in the red part of the profile may indicate the presence of movement of the substance to the observers. Note that there is no direct connection between the appearance of emission details of the line profiles and the motion of the matter of the stellar wind from the star and toward the star. Many features of the variations in the line profiles of the studied stars can be explained in the magnetically held stellar wind model proposed by Babel and Montmerle [25].

It can be seen from Fig. 1 and Table 1, when the inverse P Cyg is observed in the line Hα the profile of Hβ also changes by the structure and the value and the line radial velocity shifts to the red side and is equal to 10 km s^{-1}. It is interesting that when the inverse P Cyg is observed in Hα, no change is observed

in the line HeI (5876 Å). This indicates that in the case of inverse P Cyg profile, the event substance can reach the layers of the occurrence of the line Hβ, but does not reach the layers where the line HeI is formed.

As we see see from Table 1, during the inversion event, the half-width and the equivalent width near the line Hα decrease, and the residual intensity increases. At the same time, in the line Hβ the half-width decreased, the residual intensity increased, and the equivalent line width increased too. It can also be seen from Table 1 that the spectral parameters of the line HeI (residual intensity and equivalent width) do not show appreciable changes.

The spectrum obtained on 09/11/2014 shows that the red wing of the line Hα has a weak emission component (Fig. 1). When comparing, it was found out that in this case the lines Hα and Hβ strongly shifted to the violet side of the spectrum and the radial velocity became larger than in 11.11.2006 (Fig. 1 and Table 1). For the lines HeI (5876 Å) and doublet NaID did not observed any significant changes. Unfortunately, due to the lack of observational material, we cannot reveal a certain pattern.

HD187982. It is a supergiant star of the spectral class A21Ia [26]. The Hα line is of the PCyg type profile.Bassed on the spectra obtained ,the profiles of the lines Hα, Hβ, HeI (5876Å), doublet NaID , and FeII (4924, 5018, 5169 Å) were studied .The radial velocities ,residual intensities, and half-widths of the lines are determined. In the spectra of the star HD187982, obtained in 01.09.2013 and 06.09.2013, the profiles of the Hα lines consist of a strong absorption and weak emission component, which is observed on the red wing of the line Hα (Fig. 4). But in the spectra obtained in 02.10.2013 and 03.10.2013 the Hα line is purely absorption and there are no associated components. Although on the red wing of the absorption line of Hα the rudiments of the emission component are still visible and it does not descend to the level of the continuous spectrum. As can be seen from Fig. 4, in all these cases no structural change is observed in the profiles of the line Hβ. If we follow the values of the radial velocities Hα, Hβ, HeI and the doublet of NaId, we see that the radial velocityof Hα varies, but in this change there is no regularity that attracts attention.

It was found that the change in the radial velocity of the lines Hα and Hβ shows an interesting similarity. As was emphasized above, in the spectra of the star HD187982, the profile of the line Hα is observed in two forms:

a) The profile of the line Hα consists of a strong absorption and weak emission component, which is observed on the red wing of the line Hα (for example: 01.09.2013 and 06.09.2013).

b) The profile of the line Hα is observed in the absorption, with the presence of a weak emission component. (for example: 03.10.2013, etc.)

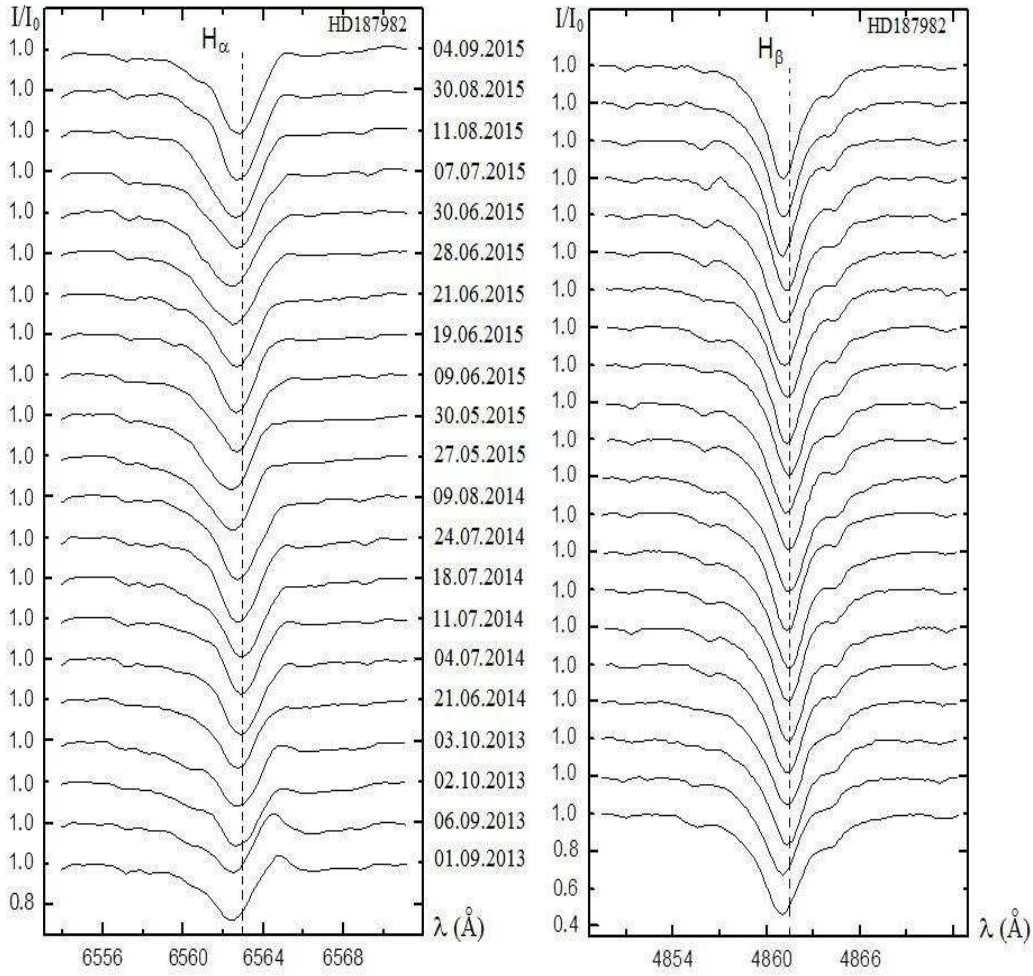

Fig. 4. The profiles of the Hα and Hβ lines in the spectrum of the supergiant HD187982, obtained at different times.

The radial velocities of the line Hβ, measured from the spectrograms obtained in 01.09.2013, 06.09.2013, 02.10.2013 and 03.10.2013 were, respectively, -33 km s^{-1}, -33 km s^{-1}, -18 km s^{-1} and -19 km s^{-1}. As can be seen, when passing the profile from the form a) to the form b) the line of Hβ the line moves to the red

Table 2. Results of the measurements of the radial velocity and spectral parameters of the lines H$\alpha$and Hβ of the supergiant star HD187982.

Date	JD 2450000 +	HD187982											
		Hα abs				Hα em				Hβ			
		Vrkms^{-1}	W Å	$\Delta\lambda_{1/2}$ Å	R	Vrkms^{-1}	W Å	$\Delta\lambda_{1/2}$	r_v	Vrkms^{-1}	W Å	$\Delta\lambda_{1/2}$	R
01.09.2013	6537.21	−29	0.89	2.5	0.28	79	0.02	0.58	1.04	−33	2.46	3.1	0.53
06.09.2013	6542.20	−23	0.77	2.6	0.24	70	0.03	0.72	1.04	−33	2.26	3.2	0.52
02.10.2013	6568.21	−18	1.29	2.9	0.31	–	–	–	–	−18	2.40	3.0	0.57
03.10.2013	6569.23	−17	1.33	2.6	0.32	–	–	–	–	−19	2.42	3.2	0.55
21.06.2014	6830.36	−11	1.06	2.3	0.33	–	–	–	–	−16	2.35	2.9	0.58
04.07.2014	6843.34	−5	1.15	2.3	0.37	–	–	–	–	−9	2.53	2.7	0.61
11.07.2014	6850.29	−6	1.10	2.1	0.37	–	–	–	–	−13	2.41	2.7	0.60
18.07.2014	6857.38	−5	1.33	2.5	0.38	–	–	–	–	−8	2.57	3.0	0.62
24.07.2014	6863.30	−12	1.36	2.4	0.41	–	–	–	–	−14	2.41	2.7	0.63
09.08.2014	6879.29	−13	1.38	2.6	0.41	–	–	–	–	−12	2.80	3.2	0.61
27.05.20154	7170.36	−24	1.30	2.9	0.36	–	–	–	–	−6	2.31	2.9	0.59
30.05.2015	7173.35	−30	1.29	2.9	0.36	–	–	–	–	−14	2.28	2.8	0.58
09.06.2015	7183.47	−17	1.23	2.7	0.37	–	–	–	–	−5	2.20	2.7	0.59
19.06.2015	7193.45	−19	1.15	2.3	0.38	–	–	–	–	−15	2.42	2.7	0.62
21.06.2015	7195.43	−16	1.22	2.5	0.36	–	–	–	–	−14	2.34	2.8	0.58
28.06.2015	7202.36	−25	1.29	3.1	0.36	–	–	–	–	−23	2.45	2.9	0.60
30.06.2015	7204.31	−27	1.36	3.2	0.37	–	–	–	–	−25	2.31	3.0	0.57
07.07.2015	7211.34	−16	1.48	3.2	0.39	–	–	–	–	−18	2.13	2.6	0.60
11.08.2015	7246.29	−19	1.59	3.0	0.44	–	–	–	–	−33	1.98	2.5	0.62
30.08.2015	7265.40	−14	1.39	2.4	0.44	–	–	–	–	−30	2.23	2.6	0.61

side, as a result, the radial velocity changes sharply, but no significant changes occur in the spectral parameters (W, R, $\Delta\lambda_{1/2}$) (Table 2).
In addition, with such a transition, the equivalent the width of Hα increases, but no significant changes occur in the values of the half-width and residual intensity. There are no noticeable changes in the radial velocities and other spectral parameters of the HeI and NaID doublet.

The next spectra of this star were obtained between 21.06.2014-09.08.2014 and 27.05.2015-04.09.2015 (Table 2 and Table 3). In the spectra, obtained in the

Table 3. Results of the measurements of the radial velocity and spectral parameters of the lines HeI, NaI and FeII of the supergiant star HD187982.

Date	2450000 +	HD187982								
		HeI				NaI D1	NaID2	FeII4924Å	FeII5018Å	FeII5169Å
		Vr kms^{-1}	WÅ	$\Delta\lambda_{1/2}$	R	Vr kms^{-1}	Vr kms^{-1}	Vr kms^{-1}	Vr kms^{-1}	Vr kms^{-1}
01.09.2013	6537.21	−1.0	0.22	1.3	0.14	−6.4	−8.0	−12.2	−10.4	−8.0
06.09.2013	6542.20	−4.7	0.19	1.5	0.11	−12.1	−13.0	−19.3	−16.8	−13.5
02.10.2013	6568.21	−2.3	0.17	1.3	0.11	−4.4	−6.5	−5.2	−7.0	−2.5
03.10.2013	6569.23	−1.5	0.19	1.4	0.12	−2.5	−3.4	−8.3	−5.7	−2.3
21.06.2014	6830.36	1.1	0.21	1.4	0.13	−10.1	−9.4	0.1	3.4	−5.6
04.07.2014	6843.34	2.7	0.18	1.3	0.13	−8.1	−7.3	−0.4	1.0	−4.9
11.07.2014	6850.29	4.1	0.21	1.5	0.13	−10.8	−9.5	−1.8	0.4	−7.8
18.07.2014	6857.38	1.7	0.25	1.4	0.14	−8.7	−8.1	1.7	1.5	−6.2
24.07.2014	6863.30	−0.4	0.21	1.4	0.12	−10.2	−9.7	−3.1	−0.5	−6.3
09.08.2014	6879.29	2.6	0.21	1.4	0.13	−5.0	−4.5	5.1	−1.2	0.5
27.05.2015	7170.36	2.0	0.23	1.4	0.13	−13.3	−12.2	6.2	4.6	4.1
30.05.2015	7173.35	1.0	0.22	1.4	0.13	−14.0	−12.0	2.1	1.0	0.8
09.06.2015	7183.47	0.0	0.21	1.5	0.12	−12.7	−11.8	−0.9	−3.3	−5.8
19.06.2015	7193.45	9.4	0.19	1.5	0.11	−15.0	−11.6	−2.8	−8.0	−6.2
21.06.2015	7195.43	8.3	0.21	1.6	0.11	−14.0	−10.8	−0.8	−2.4	−2.2
28.06.2015	7202.36	6.6	0.22	1.5	0.13	−12.9	−10.8	5.7	4.0	3.2
30.06.2015	7204.31	−1.0	0.23	1.7	0.12	−12.9	−11.0	11.4	8.8	8.7
07.07.2015	7211.34	5.9	0.23	1.4	0.14	−11.4	−10.0	−1.3	−5.2	−4.0
11.08.2015	7246.29	2.0	0.22	1.4	0.13	−12.4	−11.4	−3.9	−6.8	−6.5
30.08.2015	7265.40	3.7	0.21	1.4	0.13	−10.8	−12.9	10.0	8.1	6.4
04.09.2015	7270.39	5.4	0.19	1.4	0.13	−10.0	−12.4	9.7	8.2	7.5

period of 21.06.2014-09.08.2014 and 27.05.2015-04.09.2015 the radial velocities of Hα varied on average by ± 4 km s^{-1} and ± 8 km s^{-1}, respectively. A change in the radial velocity of $H\beta$ is on average ± 4 km s^{-1} and ± 14 km s^{-1}, respectively (Table 2).

In the lines of HeI and the doublet NaID, the variation of Vr is weak. Since, the radial velocity varies in the interval $-4.7 \div 9.4$ km s^{-1} and $-15 \div -2.5$ km s^{-1},

respectively. No significant change in the structure and the spectral parameters of the HeI lines and the doublet NaID lines were observed (Table 3). However, changes in the radial velocity of the line HeI and the doublet NaID lines sometimes exceed the measurement accuracy by several times. This means that the change is real.

In 2013-2015 the amplitude of the radial velocity variation was $\Delta Vr = (-4.7 \div 9.4)$ km s^{-1}, and the average radial velocity was Vr (HeI)$_{ave}$=2.2 km s^{-1}. Since the radial velocity of the center of mass of the star is noticeably smaller (-2.9 km s^{-1}, see Wilson 1953 [27]), it turns out that the layers where HeI absorption are formed, radial vibrations fall to the center with a speed of about 2.2-(-2.9) = 5.1 km s^{-1}. We note that this velocity changes with time, and, apparently, the amplitude also changes with its increase. The time variation of the radial velocity, equivalent to the width and depth of the lines Hα and Hβ, as well as the radial velocity of the lines HeI and FeII, is shown in Fig. 5.

Fig. 5 shows that in 2013, 2014 and 2015, the change in the radial velocity and the depth of the Hα and Hβ lines occur almost synchronously.In 2014, changes of the equivalent width of these lines vary synchronously. However, in 2015 the change occurs in anti-phase. According to our data, in 2013, the equivalent width of the Hβ line remained within the error or almost unchanged.

Our investigations show that the radial velocities of the lines FeII vary with time (Fig. 5). As can be seen from Fig. 5, especially in 2015, there are quasi-periodic changes in the values of the radial velocity in FeII line.
We note that the FeII lines present in the spectra of star HD187982 were studied in detail by Abtom, White and Hendry [26,28,29]. In Abt's work [28], based on the FeII line (4508, 4515, 4520, 4522 Å), 7.7-day quasiperiodic changes were found for radial velocities. After Abt, measurements were carried out by Hendry [26]. He added his measurements to the result of White [29] and Abta and obtained the same previously found 7.7-day period.

On the basis of the spectograms curves of the changes in the radial velocities obtained from the lines FeII were plotted (Fig. 6). Fig. 6 shows that, according to our data, 7.7-day periodical changes have not been confirmed.

The amplitude of the radial velocity for Hα and Hβ increases, reaching $\Delta Vr = (-30.0 \div -5.0)$ and $(-33.0 \div -5.0)$ km s^{-1}, respectively. The average values of the radial velocities for Hα and Hβ are -17 and -18 km s^{-1}, which indicate a systematic expansion of the corresponding layers relative to the lower and intermediate layers.

Comparison of amplitudes and average velocities found for different layers shows that all these parameters depend to some extent on the optical depth of their formation in the atmosphere. Similar dependences for α Cyg (A2Ia) were found by Inoy [30], and for RH21389 by Rzayev and Chentsov [31].

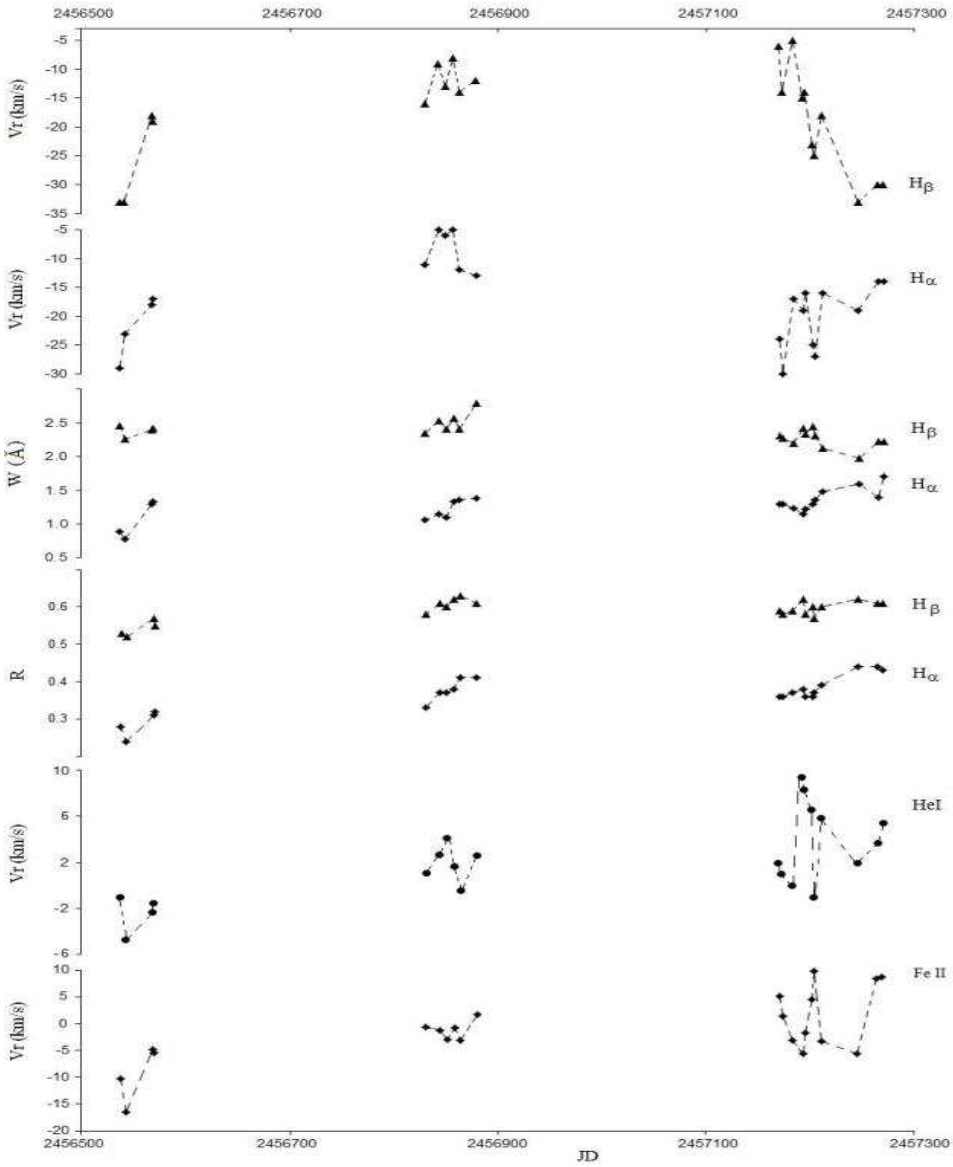

Fig. 5. Changes with time the radial velocity, equivalent width and depth profiles of the lines Hα, Hβ and the average radial velocity measured for the HeI and FeII lines in the spectrum of the supergiant HD187982.

So, the analysis of long series of observations of HD187982 from 2013 to 2015 showed that the amplitude and the average value of the radial velocities differ for the different layers. The lower and intermediate layers fall on the star with a

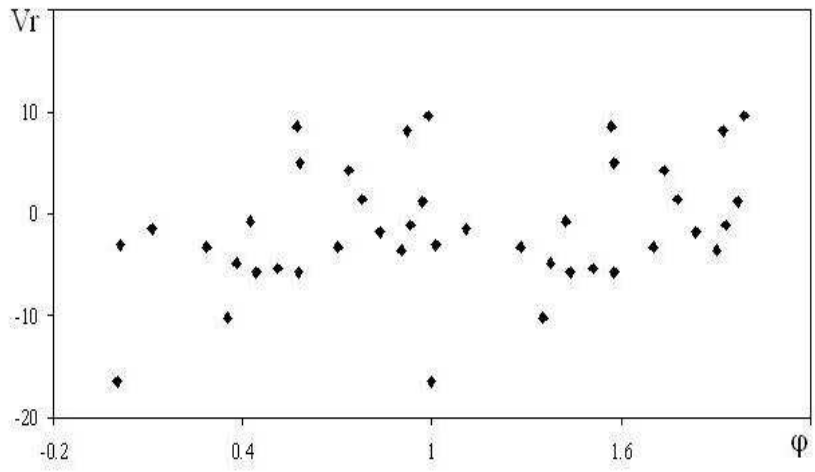

Fig. 6. Changes in the radial velocities V_r from the phase obtained from the FeII lines in the spectrum of the supergiant HD187982 (the initial epoch was chosen JD2456542.2, P = 7.7 days).

velocity of 5.1 and 1.9 km s^{-1} while the upper layers expand.

The sodium doublet NaI 5890 Å and NaI 5896 Å. In the spectrum of the stars HD 21389 and HD187982, in addition to hydrogen and other lines, the lines of the doublet NaI 5890 Å and NaI 5896 Å have also been studied.

It is known that the absorption lines of NaI 5890 Å and NaI 5896 Å are mainly interstellar lines, i.e. are formed in the interstellar medium. Therefore, the profiles of these lines must be symmetrical. The asymmetry of these profiles is an argument in favor of the contribution of other sources to the formation of these lines.

A study of the optical spectra of these stars, as well as of other hot supergiant stars, obtained by us and other authors, indicate that in the formation of the doublet NaID, in addition to the star, the envelopes around these stars and the interstellar medium can also contribute. Unfortunately, because of the small resolution in the spectrum, we could not identify these components. However, in 11.11.2006 the asymmetry in the violet wings of these lines was observed in the profile of the doublet NaID in the spectrum of HD 21389 (Fig. 2-3). Therefore, to reveal asymmetry, we combined the red wing of these lines with the Gaussian profile [24]. In Fig. 2 and Fig. 3, the dashed line shows the alignment of the red wing with the Gaussian profile [24].

The radial velocities of the lines are determined by combining the direct and mirror images of these absorption lines at the half-depth level Vr (R/2), and also in the peaks of the profiles. Laboratory wavelengths (D2, D1) were taken as 5889.95 Å and 5895.92 Å, respectively. The radial velocities and equivalent widths (W) determined by us are given in Table 1.

As can be seen from Table 3, the radial velocities and equivalent widths of the absorption lines of NaI 5890 Å and NaI 5896 Å determined by us in the spectrum of these stars do not change significantly, except 04.09.2015 one in the spectrum of the supergiant HD 187982. In addition, only in 11.11.2006, the asymmetry is observed in NaID doublet line,in the spectrum of HD21389.

The appearance and disappearance of the asymmetry in the profile of doublet NaID and the formation of the profile of inverse P Cyg type of Hα line in the atmosphere of the supergiant HD21389 occur synchronously (Fig. 1,2).

We assume that these changes formed under the action of a general mechanism, which are the cause of pulsation and the outflow of the matter from the stellar atmosphere.

3. DISCUSSION OF THE OBTAINED RESULTS

Summarizing the observational data and the measurements made, the following conclusions can be drawn:

It is known that the line Hα, in relation to other lines, covers the higher layers of the atmosphere [32], since in the supergiant stars the upper layers of the atmosphere are subjected to the higher effect, than the lower layers. The change in the radiation flux of the star and the outflow of the matter (stellar wind) creates a corresponding change in the upper layers of the atmosphere and in the envelope. As a result, the profiles of the absorption and emission components change, and appear in the different forms. That is, changes in the profiles of the line Hαin the spectra of HD21389 and HD187982 can be the result of the release of matter and perturbation of the envelope.

On the other hand, it is known that the appearance of the stellar wind and its variation in the supergiant stars is associated with the pulsations occurring in their atmosphere [33]. But, if these changes are associated with pulsations, then they should occur periodically. In order to clarify the nature of physical processes in the deep layers of the atmosphere, it is planned to carry out regular spectral and photometric observations of this star in the future.

As noted above, the asymmetry in the interstellar absorption lines of NaI 5890 (D2) and NaI 5896 (D1) in the spectrum of the supergiant HD 21389 (Fig. 2,3) is revealed. This asymmetry is observed in the violet wings of these lines only on

11.11.2006, when the Hα line is observed in the shape of the inverse PCyg profile. But we could not detect the asymmetry in the profile of the doublet NaD in the spectra of the supergiant HD187982. This observational fact is an additional argument in favor of the reality of the asymmetry of the investigated absorption lines of NaI 5890 (D2) and NaI 5896 (D1) in the spectrum of the star HD 21389.

We assume that the observed changes can be explained by the macroscopic radial motions or semiregular or irregular movements like pulsations [16, 18].

Our investigations showed that all the measured parameters of the lines Hα, Hβ, and FeII in the star HD187982 obtained in $2013 \div 2015$ show variability for a month or less. The change occur sometimes synchronously or sometimes in anti-phase.

The appearance of PCyg profile on the spectrograms on 01.09.2013 and 06.09.2013 indicates the discovery of the star of the supergiant HD187982 in the next active stage. The spectrograms obtained after 06.09.2013 show a decrease in the intensity of the emission component, which is accompanied by a decrease in the radial velocities in the lines Hα, Hβ and FeII These facts indicate that, a powerful outflow of matter occurs, the physical conditions the velocity and direction of the outflow change in the atmospheric layers of the supergiant star , where these lines are effectively formed.

CONCLUSIONS

As a result of the comparative analysis of the Hα absorption lines in the spectrum of the supergiant stars HD21389 and HD187982 obtained in 2005-2015 by us , we can come to the following conclusions:

1. In the spectrum of HD21389, the absorption profile of the Hα line in dependence on the instability phase of the star atmosphere is of a complex structure. In the active phase this line has an inverse P Cyg profile. Emission components appear and disappear in the red and violent wings of the profile. All the measured parameters of the Hα line show variability. It is assumed that the variability of the profiles, radial velocities and other parameters are related to each other as a result of the outflow of the matter and perturbation of the envelope , as well as pulsations and stellar winds produced in the atmosphere of the stars.

2. The appearance and disappearance of the asymmetry in the profile of doublet NaID and the formation of inverse P Cyg tpe of Hα line in the atmosphere of the supergiant HD 21389 occurs synchronously (Fig. 1, 2). We suggest that the observed changes can be explained by the macroscopic radial motions or by semiregular or irregular pulsating motions [16], [18].

3.The absorption profile of the Hα line has a complex structure in the spectrum of the supergiant star HD187982. This line has a normal P Cyg profile in

the active phase. Emission components appear and disappear in the red wing of the profile. All the measured parameters of the lines Hα, Hβ and FeII 2013$\div$2015 show variability for a month or less.Sometimes changes occur either synchronously, and sometimes occur in antiphase.

We consider that these results can be used for the further analysis of the chemical composition and the determination of the fundamental parameters of the atmosphere, and also for constructing the theoretical model of this star.

REFERENCES

1. V.Straizys and V.Laugalys, Young stars in the camelopardalis dust and molecular clouds. I. The Cam OB1 association, Baltic Atronomy, 2007, v. 16, p.167-182.

2. Y. Takeda and Masahide Takada-Hidai, Oxygen abundances in late – B through F supergiants, Japan Astronomical Society, 1998, v. 50, p. 629-638.

3. E.Verdugo, A.Talavera and A.I.Gomez de Castro, Understanding A-type supergiants. II. Atmospheric parameters and rotational velocities of Galactic A-type supergiants, Astronomy and Astrophysics, 1999, v. 346, p. 819-830.

4. C. de Jager, H. Nieuwenhuijzen and K.A. van der Hucht, Mass loss rates in the Hertzsprung – Russel diagram, Astronomy and Astrophysics, Supplement Series, 1988, v. 72, p. 259-289.

5. Y. Takeda and Masahide Takada-Hidai, Helium and Carbon abundances in late – B and early – A supergiants, Japan Astronomical Society, 2000, v. 52, p. 113-125.

6. L.Achmad, H.J.G.L.M.Lamers and L.Pasquini, Radiation driven wind models for A, F and G supergiants, Astronomy and Astrophysics, 1997, v. 320, p. 196-208.

7. A.Talavera and A.I.Gomez de Castro, The UV high resolution spectrum of A - type supergiants, Astronomy and Astrophysics, 1987, v. 181, p. 300-314.

8. E.B. Zvereva, S.K. Zeynalov, E.L. Chentsov, On the systematic movements of matter in the atmospheres of white supergiant stars HD21291 and HD21389, Izv. CAO, 1984, v. 18, c. 29-36.

9. S.K. Zeynalov, Nonstationary phenomena in the atmosphere of supergiant stars O, B, A, F, Doctoral dissertation, Tbilisi, 1997.

10. S.K. Zeynalov, Possible periodicity and changes in the profile of the Hαline in the spectra of the stars HD21291 B9Ia and HD21389 A0Ia, ShAO proceedings, 2003, No. 106, p. 22-27.

11. A.H. Rzaev, S.K. Zeynalov, E.L. Chentsov, On systematic movements in the atmospheres of stars HD21291 and HD21389, Kinematics and physics of celestial bodies, 1989, v.5, No.1, pp.75-81.

12. E.Verdugo, A.Talavera and A.I.Gomez de Castro, Understanding A-type supergiants. I. Ultraviolet and visible spectral atlas of A-type supergiants, Astronomy and Astrophysics, 1999, v. 137, p. 351-362.

13. S.K.Zeinalov and A.KH. Rzaev, Non-stationary atmospheres of supergiants. I. Systematic movement of matter in the atmospheres of stars HD21291 and HD21389, Astrophysics and Space Science, 1990, v. 172, p. 211-216.

14. S.K.Zeinalov and A.KH. Rzaev, Non-stationary atmospheres of supergiants. II. The Hα profile variations in the spectra of HD21291 and HD21389, Astrophysics and Space Science, 1990, v. 172, p. 217-224.

15. Wm. Bruce Weaver and Ana V. Torres-Dodgen, Neural network classification of the near-infrared spectra of A-type stars, Astrophysical Journal, 1995, v. 446, p. 300-317.

16. L.Denizman and M.Hack, Spectra and radial velocities of white supergiants, Astronomy and Astrophysics, 1988, v. 75, p. 79-92.

17. R.O.Gray and R.F.Garisson, The early A type stars: Refined MK classification, confrontation with stromgren photometry, and the effects of rotation, Astrophysical Journal, Supplement Series, 1987, v. 65, p. 581-602.

18. G.Burki, The semi – period – luminosity – colour relation for supergiant stars, Astronomy and Astrophysics, 1978, v. 65, p. 357-362.

19. Evans C. J., and Howarth Ian D. Characteristics and classification of A – type supergiants in the small Magellanic cloud, Mon. Not. R. Astronomical Society, 2003, v. 345, p. 1223-1235.

20. N.Przybilla, M.Firnstein, M.F.Nieva, G.Meynet and A.Maeder, Mixing of CNO – cycled matter in massive stars, Astronomy and Astrophysics, 2010, v. 517, p. 1-6.

21. Helmut A.Abt and Nidia I. Morrell, The relation between rotational velocities and spectral peculiarities among A – type stars, Astrophysical Journal, Supplement Series, 1995, v. 99, p. 135-172.

22. R.L.Snell and P.A.Vanden Bout, High – resolution profiles of the 5780 Å interstellar diffuse band, Astrophysical Journal, 1981, v. 244, p. 844-847.

23. H.M. Mikailov, V.M. Khalilov, I.A. Alekberov. Eshelle - Cassegrain Focus Spectrometer of the 2 - meter Telescope of the ShAO of NAS of Azerbaijan, ShAO proceedings, 2005, No.109, pp.21-29.

24. GA Galazutdinov, DECH20 Spectral Spectrum Processing System, 1. Image processing. 2. Spectra processing, Preprint of CAO, 1992, No. 92.

25. J.Babel, T. Montmerle, On the periodic X-ray emission from Orionis C, The Astrophysical Journal, 1997, v.485, Issue 1, pp. L29-L32.

26. Elaine M. Hendry, Bright new spectroscopic binaries discovered from composite spectra. III. HR 233, HR 676, HR 1129, Gem, HR 7573, and HD 213470, The Astronomical Journal, 1981, v. 86, p. 1540-1545.

27. Wilson, R. E. General catalogue of stellar radial velocities, Washington, [Carnegie Institution of Washington] 1953 (Bibliographic Code: 1953GCRV..C.....0W)

28. Helmut A.Abt, The Variability of Supergiants, Astrophysical Journal, 1957, v. 126, p. 138-151.

29. William C. White, Radial velocities of six stars having composite spectra, Astrophysical Journal, 1950, v. 112, p. 559-560.

30. Inoue M.O. Variation in radial velocities and line profiles of Alpha Cygni (A2Ia), Publications of the Astronomical Society of Japan, v. 31, 1979, pp. 11- 21.

31. Rzaev A.Kh., Chentsov E.L., Zeynalov S.K. Spectroscopic investigation of quasiperiodic motions such as pulsations in the atmospheres of early supergiants. I. HD21389. Changes in radial velocities with time, Izvestiya Special Astrophysical Observatory, 1991, v. 34, pp.84-101.

32. K. De Jager, Stars of the highest luminosity, Moscow, Mir, 1984, 493 p.

33. J.P. Cox, Theory of Stellar Pulsations, Moscow, Mir, 1983, 326 p.

HD21389 VƏ HD187982 İFRATNƏHƏNG ULDUZLARIN SPEKTROSKOPİK DƏYİŞKƏNLİKLƏRİ

Y. M. Məhərrəmov, Ə. R. Həsənova, Ə. M. Xəlilov, Ə. Ş. Baloğlanov, G. M. Hacıyeva

N.Tusi adına Şamaxı Astrofizika Rəsədxanası, Azərbaycan Milli Elmlər Akademiyası, Şamaxı rayonu, Azərbaycan

Bu işdə, 2005-2006 və 2013-2015-ci illərdə ŞAR-da 2 metrlik teleskopunda quraşdırılmış kasseqren fokusunda CCD işıqqəbuledicisi ilə HD21389 və HD187982 ifratnəhəng ulduzlarının alınmış spektrlərinə əsasən Hα, Hβ, HeI (5876 Å) və dublet natrium NaID xətləri profillərinin quruluşu, onlarda şüa sürətləri və spektral parametrləri tədqiq olunmuşdur. Aşkar olmuşdur ki, HD21389 ulduzu spektrində Hα xətti profilinin quruluşu ulduz atmosferinin aktiv fazasından asılı olaraq mürəkkəb quruluşa malikdir. Aktiv fazada xəttin profili invers P Cyg tiplidir. Hα xəttinin qırmızı və bənövşəyi qanadında şüalanma komponenti yaranır və yox olur. Hα və Hβ xətlərinin bütün ölçülmüş parametrləri dəyişkənlik göstərir. HD21389 ifratnəhəng ulduzu atmosferində dublet natrium xəttinin profilində asimmetriyanın yaranması və yox olması Hα xəttinin profilinin invers P Cyg profilə çevrilməsi ilə sinxron baş verir. HD187982 ifratnəhəng ulduzu spektrində Hα profilinin qırmızı qanadında şüalanma komponenti yaranır və yox olur. Ulduz atmosferinin aktiv fazasında bu xətt normal P Cyg profili formasındadır. 2013-2015-ci illərdə Hα, Hβ və FeII xətlərinin bütün ölçülmüş parametrləri (Vr, W, R) bir ay və daha qısa müddətdə dəyişkənlik göstərir. Parametrlərin dəyişməsi bəzən sinxron, bəzən də əks fazada baş verir. Bütün bu faktlar onu göstərir ki, HD187982 ulduzu atmosferinin tədqiq olunan xətlərinin formalaşdığı müəyyən effektiv qatlarda maddə axını baş verir, axının sürəti və istiqaməti dəyişir, pulsasiya tipli hərəkətlər müşahidə olunur.

Açar sözlər: İfrat nəhəng ulduzlar – Pulsasiya